HYBRID RENEWABLE ENERGY SYSTEM WITH WIND

TURBINE AND PV PANELS

A Thesis
Submitted to The Graduate Faculty
of the
North Dakota State University
of Agriculture and Applied Science

By

Munir Shabir Kaderbhai

In Partial Fulfillment of the Requirements
for the Degree of
MASTER OF SCIENCE

Major Department:
Electrical and Computer Engineering

April 2010

Fargo, North Dakota

North Dakota State University
Graduate School

Title

Hybrid Renewable Energy System with Wind Turbine and PV Panels

By

Munir Kaderbhai

The Supervisory Committee certifies that this ***disquisition*** complies with North Dakota State University's regulations and meets the accepted standards for the degree of

MASTER OF SCIENCE

ABSTRACT

Kaderbhai, Munir Shabir, M.S., Department of Electrical and Computer Engineering, College of Engineering and Architecture, North Dakota State University, April 2010. Hybrid Renewable Energy System with Wind Turbine and PV Panels. Major Professor: Dr. Subbaraya Yuvarajan.

In recent years, there has been increasing concern about the world's heavy dependence on fossil-based fuels and the pollution caused by such fuels. This has sparked an increased interest in the use of other renewable sources of energy. In particular, electricity generation from wind and photovoltaic energy has seen a rapid growth in recent years. One of the most widely used electric machines used in wind energy conversion systems is the doubly-fed induction generator (DFIG) which requires a source and power converter system to feed variable frequency AC voltage to its rotor. Power converter schemes currently used with DFIGs, however, do not address issues such as the absence power factor correction in the rectifier (without complicated control loops), soft-switching in the rectifier, and the possibility of integrating photovoltaic power into the system to provide rotor injection power.

This thesis presents a hybrid system in which the rotor power can be drawn either from three-phase AC mains or a photovoltaic (PV) panel-battery combination. While drawing power from AC mains, an AC-DC converter with soft switching and power factor correction is used. While supplying rotor injection power from PV panels, one of the MOSFET switches of the AC-DC converter will be used for boosting the PV panel output voltage. Various stages of the system are implemented and the details of implementation and results are discussed for each stage. Suggestions for future research are also offered.

ACKNOWLEDGEMENTS

TABLE OF CONTENTS

LIST OF TABLES

LIST OF FIGURES

CHAPTER 1. INTRODUCTION

As the world's stocks of "dirty" fossil fuels decline at an alarming rate at the same time as our demand for energy increases, the need for alternative clean and sustainable sources of energy is clearly evident. Sources of renewable energy (RE) such as wind and solar are gaining increased popularity as viable sources of energy that can provide power on a large scale both cleanly and economically.

1.1. Wind Energy Systems

In wind energy systems, a wind turbine converts wind kinetic energy into electrical energy. The energy conversion system typically consists of wind blades which are coupled to the rotor shaft of an electric generator. The generator power is proportional to the speed of the rotor shaft and this means that fluctuations in wind speed can cause changes in the voltage frequency and magnitude. Power grids, however, require electrical power at a constant frequency. Hence, power electronic converters are integral part of these energy systems, being able to convert generated electricity into consumer usable and utility compatible forms.

One type of wind turbine is fixed speed, where the generator shaft rotates at a constant speed. However, fixed speeds systems are not capable of harvesting all the wind's energy at high speeds and are often required to be shut down at low speeds. To obtain optimal energy conversion, variable speed turbines are used, where the generator shaft speed is allowed to vary proportionally to the wind speed. Variable speed wind turbines, however, require complicated and expensive power converters and turbine control.

In variable speed systems, the most commonly used generator is the doubly-fed induction generator (DFIG). This system uses a wound-rotor induction machine to convert the mechanical power from the wind turbine into a fixed-frequency AC output supplied to the grid. The frequency of the voltage injected into the rotor is adjusted such that the sum of rotor frequency and the equivalent frequency corresponding to mechanical rotation is equal to the desired stator frequency (60Hz). In this scheme, the power required for rotor injection is a small fraction of the output power and it comes from the AC mains through a set of power converters. Thus the system uses power converters as well as filters with correspondingly lower ratings.

Some of the issues not addressed by the existing DFIG control schemes are: (a) the absence of power factor correction in the rectifier (b) the absence of soft switching that could improve the efficiency of the rectifier and (c) the ability to supply AC power to isolated loads preferably using another power source. As for (c), PV panels installed alongside the wind turbine can be used to aid wind generation.

1.2. Hybrid Scheme and Power Electronics

This thesis proposes a hybrid scheme in which the injection power can be drawn from (a) AC mains at unity power factor if available or (b) a set of PV panels and a back-up battery in the absence of AC mains [I]. The three-phase power from the AC mains is converted into a DC using a three-phase resonant-boost power factor corrector (PFC) with only two switches implementing zero voltage switching (ZVS). In the absence of the AC bus, a set of PV panels supply injection power to the rotor through a boost converter which is realized using one or more of the switches in the power factor corrector. Thus, a separate power converter is not required for the PV panels. This helps to reduce the cost of the

2

overall system and also increases reliability by decreasing the number of components in the system. A battery is added as (a) a buffer storing the extra energy from the PV panel when the maximum power available is more than what is required for rotor injection and (b) a DC source providing injection power in the absence of sunlight. The hybrid power converter system proposed is useful in combining wind energy and solar energy such that the wind energy constitutes the bulk of the power produced while the solar (PV) panels provide a fraction of the power through rotor excitation.

1.3. Scope of Work

This thesis presents a novel power converter scheme in which rotor injection to a wind energy system utilizing a DFIG power can be supplied from either the grid or another source like PV panels. The system is flexible enough so that when connection to the grid is not available, rotor injection can easily be provided by a PV panel/ battery combination. This is particularly useful in areas with an unreliable utility network, where there could prolonged periods of load-shedding or power cuts.

In addition, the system also takes into account the complementary nature of wind and solar energy. When there is enough wind to drive the DFIG, then the PV panels can be used to support the wind energy production through rotor injection. During periods of low wind speeds, when the wind turbine does not operate, the PV panels can continue to provide AC power to the network. In this case, the DFIG would simply operate as a transformer. Traditionally, hybrid schemes with wind turbines and PV panels require separate power converters for both the wind turbine and the PV panels. The hybrid scheme proposed in this thesis integrates both the wind turbine and PV panels into one power

converter scheme which helps to increase efficiency and reliability of the WES, and also helps to reduce cost.

1.4. Outline of Thesis

Chapter 2 introduces various sources of RE. Since the work in this thesis involves wind and solar energy, these two sources are introduced. Basic principles of wind energy conversion, including the types of wind turbines are discussed. Next, the characteristics of PV panels are discussed along with a review of some of the more commonly used maximum power point (MPP) tracking techniques used in PV applications.

Chapter 3 reviews power converters for wind and solar RE systems. This chapter first reviews the relationship between power factor (PF), distortion and total harmonic distortion (THD). Next, a review of various configurations of power converter systems used in wind energy systems utilizing DFIGs is presented. This is followed by a brief discussion about DC/DC converters used in PV applications.

Chapter 4 presents the novel hybrid DFIG-based wind energy system described earlier. Various stages of the system are implemented and the details of implementation and results are discussed for each stage. First, there is a general discussion about the characteristics of the PFC used in the proposed system, which is simulated using software and also implemented in hardware. Both simulation and experimental results are presented. Next, the current-based MPPT hardware implementation for PV power using a digital signal controller (DSC) is presented and experimental results are provided. This is followed by a discussion of the inverter and control of a DFIG. A slip and constant Volts/Hz control scheme is used to control the rotor injection so as to maintain the DFIG stator voltage at a constant magnitude and frequency. The scheme is tested with simulations of the hybrid

4

system and the results are presented. Next, the implementation of a DSC-based inverter controller for DFIG rotor injection is presented. The DSC is used to generate the gate signals by implementing Sine PWM entirely using software.

Chapter 5 introduces multilevel inverters, which are receiving increased attention for use in RE systems. Among the various types of multilevel inverters, it is the multilevel cascaded h-bridge inverter (MCHBI) with fundamental frequency switching that is chosen for analysis. The MCBHI could prove to be a good replacement for the Sine PWM rotor-side inverter in the DFIG system as it offers certain advantages such as the possibility of easily integrating other sources of RE into the system. Analysis is presented on how the switching angles for the MCBHI can be selected so that a fundamental voltage component of a desired magnitude can be generated while eliminating certain specifically chosen lower order harmonics.

Finally, a summary of the work done and conclusions arrived at are given in Chapter 6. Suggestions for future research are also given.

1.5. Contributions

This thesis presents a novel hybrid DFIG rotor injection scheme as previously described. In addition, a novel method for implementing maximum power point tracking of PV panels is also presented. The method used in this work is an adapted version of the work done in [13]. In this work, the switch of the boost converter itself is used to short the PV array *and* is also used to directly control the PV output current, resulting in a simpler power circuit. Further details of implementation are presented in Section 4.3. Additionally, a novel concept of a hybrid DFIG-based wind energy system utilizing a multilevel

cascaded H-bridge inverter for DFIG rotor injection is proposed. Some preliminary discussion on an implementation strategy and simulation results are presented.

CHAPTER 2. REVIEW OF ENERGY HARVESTING FROM WIND AND SOLAR SOURCES AND THEIR CHARACTERISTICS

2.1. Introduction to Renewable Energy

Today, coal, petroleum and natural gas constitute the bulk of the worlds energy supply. These non-renewable supplies are dwindling at an alarming rate and are becoming more expensive and more environmentally damaging to retrieve. Furthermore, they are a major source of greenhouse gasses such as carbon dioxide, which has been attributed to rising global temperatures, and other pollutants. This has shifted the focus back to renewable energy sources which can play a key role in producing clean and inexhaustible energy. The work done in this thesis involves both wind and solar energy. Therefore, we will explore these two sources in more detail in this chapter.

2.2. Introduction to Modern Wind Power Conversion

2.2.1. Basic Principles in Wind Energy

There has been a steady growth in the development of wind energy conversion systems (WECs) over the past 25 years [2]. A typical wind turbine is illustrated in Figure 2-1 and it includes the turbine rotor, gearbox, generator, transformer, and in some cases power converter stages.

The function of a wind turbine is to convert the linear kinetic energy of the wind to rotational energy that can be used to drive a generator. The power from the wind is

captured by means of aerodynamically designed blades and is converted into rotary mechanical power. Wind turbines can be classified into vertical axis wind turbine (VAWT) or horizontal type wind turbine (HAWT). Most modern wind turbines use a horizontal axis configuration and typically have three blades [3].
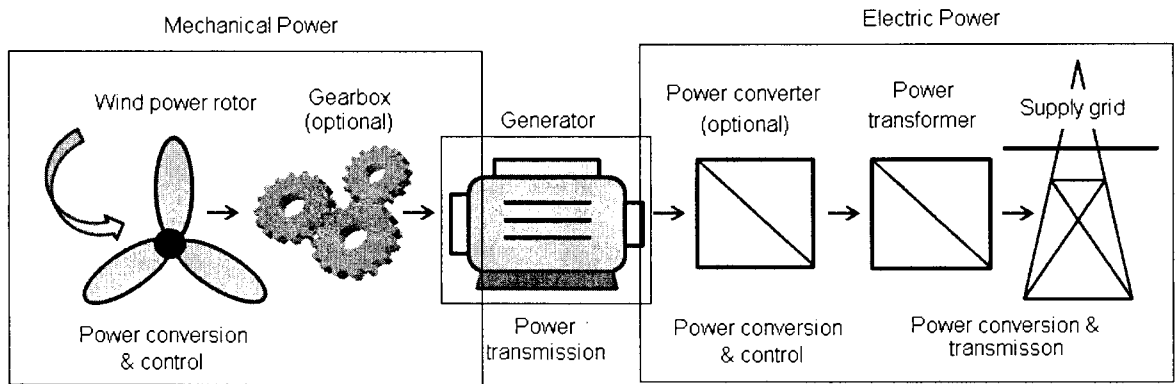
Figure 2-1: Conversion of Wind Energy to Electrical Energy in a Wind Turbine

The amount of power captured from a wind turbine is specific to each turbine and is given by [3]:

$$P = \frac{1}{2}\rho\pi R^2 v^3 C_p \tag{2.1}$$

where P is the turbine power, ρ is a the air density, v is the wind speed, R is turbine radius, and C_p is the coefficient of performance of the wind turbine. The coefficient of performance of a wind turbine is influenced by the tip-speed to wind speed ratio (TSR) given by [3]:

$$TSR = \frac{\omega R}{v} \tag{2.2}$$

where ω is the rotational speed of the turbine and R is the turbine radius. Figure 2-2 shows a typical curve which relates C_p to the TSR and shows that there is one specific TSR where the wind turbine is most efficient [4]. The maximum possible theoretical value of Cp,

referred to as the Betz limit, is equal to 16/47 ≈ 59 %. In order to achieve optimal power, the TSR should be kept at the optimal value for all wind speeds so as to operate with the highest C_p value. This can only be achieved by a variable-speed wind turbine which will adjust the rotor speed with varying wind speed, up to rated power, so as to keep TSR constant at the optimal level. Modern wind turbines for electricity generation operate at C_p values of about 0.4 [5].
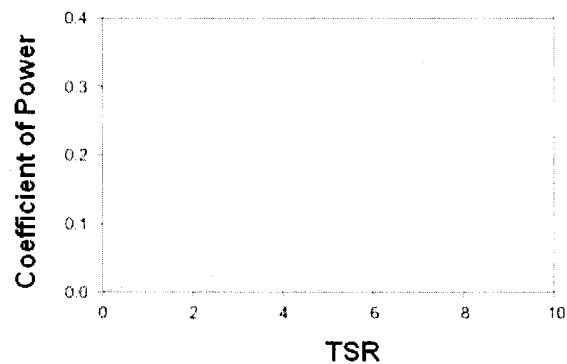
Figure 2-2: Typical Coefficient of Power Curve

2.2.2. Current Wind Turbine Technology

Wind turbine systems can be broadly classified as *fixed-speed* or *variable-speed* systems, and induction generators can be used in either system. Synchronous generators, on the other hand, are used in variable-speed systems utilizing some sort of power electronics interface. The two systems will be briefly discussed in this section.

Fixed-Speed Wind Turbines

The early wind turbines, installed in the 1990's, are normally operated at fixed speed [6]. Caged rotor (or squirrel cage) induction generators are normally used in fixed-wind systems where the stator of these generators are directly connected to the grid. This

means that the grid frequency determines the rotational speed of the generator and therefore the speed of turbine rotor as well. Squirrel-cage induction machines draw really large currents on startup which can be up to 7 times the rated current. Therefore, a soft-starter is utilized to minimize transient currents during energizing. Also, the induction generator needs to be provided with reactive power from the grid and so a capacitor bank is usually installed nearby for reactive power compensation.

The advantage of using a fixed-speed wind turbine is that it allows the use of an induction machine which is simple and very robust. This makes them cheaper compared to other WT systems. The downside is that they need a stiff grid to operate properly and reactive power consumption is not controllable. Because they only operate at one speed, the mechanical construction has to be made strong enough to absorb the high mechanical stress due to wind gusts which can cause torque pulsations in the drive train and gearbox. Furthermore, these mechanical pulsations show up as fluctuations in electrical power in the grid and in weak grids, this can cause large voltage fluctuations and higher line losses.

Variable Speed Wind Turbines

Variable speed turbines are now the most common type of wind turbines. These turbines are normally connected to the grid via a power electronic system. Both induction generators and synchronous generators can be used. The three types of induction machines used are: squirrel cage, wound rotor with slip control rotor resistance, and doubly fed induction generators (DFIG) [5]. Synchronous generators can be multi-pole generators with rotor field excitation or permanent magnet generators. All types of generators are connected to the grid through a power converter that controls the generator speed. The power converters are either full-rated or fractional-rated and are connected either to the

stator or the rotor depending on the generator type. Details about power converters will be presented in Chapter 3.

Variable speed WTs are designed to operate at maximum efficiency by tracking the maximum power point over a wide range of wind speeds. As discussed earlier in this section, the rotational speed of the variable speed WT can be varied continuously so as to maintain a constant TSR and therefore an optimal C_p value. Unlike a fixed-speed system, variable speed systems effectively absorb the wind gusts.

The variable-speed wind turbines offer several advantages when compared to the fixed speed systems. They are able to capture more energy by tracking maximum power. Also they are not subjected to high mechanical stresses due to wind gusts and this translates to a better power quality. The main disadvantage of a variable speed system is that it requires more components and complicated control strategy which makes the system more expensive. Furthermore, the use of power electronics results in additional losses in the system.

Today the most commonly used variable speed WT configuration is the doubly fed induction generator (DFIG). Since a DFIG is used in this project, further discussion is warranted and is presented in the next section.

Doubly Fed Induction Generator (DFIG)

The DFIG is a wound rotor induction machine where the rotor windings are externally accessible. Figure 2-3 shows a schematic of a typical wind energy system utilizing a DFIG. The stator windings are directly connected to the grid and the rotor windings are connected to a bidirectional back-to-back voltage source converter. The stator voltage is applied from the grid and the rotor voltage is provided by the inverter, hence the

name "doubly-fed". Mechanical power from the wind turbine is converted into a fixed frequency and magnitude AC output supplied to the grid. The frequency of the current injected into the rotor is adjusted such that the sum of rotor frequency and the equivalent frequency corresponding to mechanical rotation is equal to the desired stator frequency (60Hz). The system allows the speed of the generator to vary by ±33 % about the synchronous speed [7].
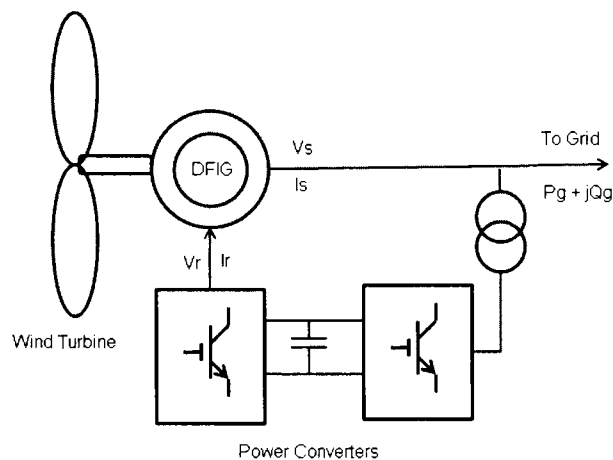
Figure 2-3: Doubly Fed Induction Generator (DFIG)

The power converter used in a DFIG consists of a rotor side converter and a grid side converter and each is controlled separately. Typically the rotor side converter controls the amount of active and reactive power of the system by controlling the rotor current components and the grid-side converter maintains a constant DC link voltage [6]. The power converters as well as filters need only be partially rated to about 25 % of the total system power which means reduced cost. The stator always feeds power into the grid. Under sub-synchronous, conditions power is fed into the rotor via the power converters. Under super-synchronous conditions, the rotor power flow is reversed and flows out of the

12

rotor and is fed into the grid via the converters. The rotor power (P_r) and stator power (P_s) are related by $P_r = s*P_s$ where s is the slip.

There are several advantages of using a DFIG. A soft starter is not required and active and reactive power can be controlled. Furthermore, the DFIG can either produce or absorb reactive power from the grid to assist with the task of voltage control in the case of a weak grid [6]. The disadvantage of a DFIG is that it needs a wound rotor with slip rings.

2.3. Introduction to Solar Power Conversion

2.3.1. Basic Solar Photovoltaic Characteristics

The function of solar photovoltaics (PV) is to convert solar energy directly into electrical energy. A single converter cell is called a solar cell or a photovoltaic cell. Several solar cells can be combined to increase power output and this is called a solar module or an array. The cells are made up of semiconductor materials which generate electricity by means of the photovoltaic effect [9].

Each individual solar cell will produce around 0.5V with a current that is proportional to the area of the cell. Solar cells are typically combined into modules of about 40 cells and the individual cells are connected in series-parallel combination to meet the voltage, power and reliability requirements. About 10 modules are combined to form a PV panel and panels providing as much as 300W each are commercially available today.

The current–voltage (I-V) characteristic is nonlinear and is given by [9]:

$$I = I_L - I_D \left[e^{\frac{QV_{OC}}{AKT}} - 1 \right] \tag{2.3}$$

where I is the output current, I_L is the light generated current, V_{OC} is the open-circuit voltage and T is the absolute temperature. The short circuit current of a cell, I_{SC} is almost

equal to I_L. Figure 2-4 shows a typical PV output characteristic. The figure shows the basic I-V characteristic, and power-voltage (P-V) characteristic derived from the I-V characteristic. Figure 2-4(a) shows the non-linear relationship between voltage and current and also shows how the output current depends on insolation level. Figure 2-4(b) shows how the power supplied by the PV panel varies with temperature, T. It is to be noted that the maximum power is reached only at a particular operating point Q which is called the maximum power point (MPP).
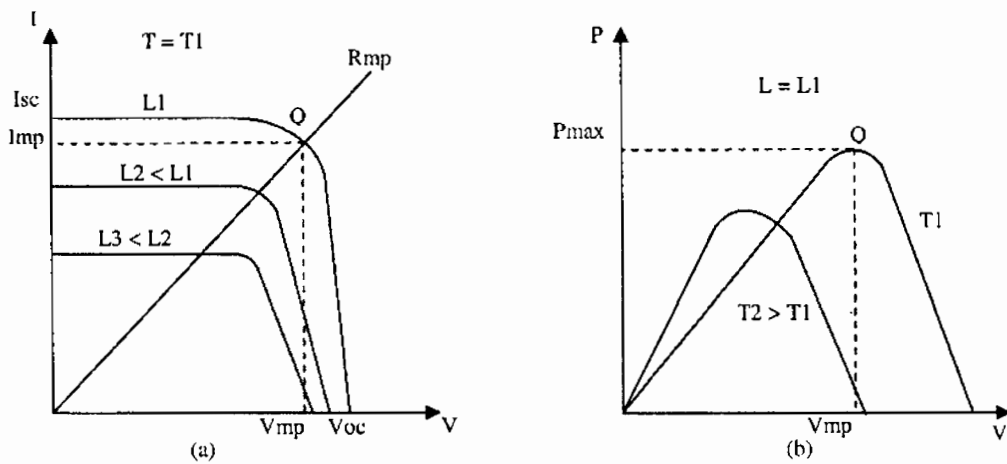
Figure 2-4: Characteristic of a Typical PV Panel (a) I-V and (b) P-V Characteristics of PV Panel at Different Insolation Levels (L) and Temperature (T)

Without any control, the PV operation could be at any operating point on the P-V curve and there is no guarantee that operation will be at the MPP. It is quite possible that the output power is very small. Furthermore, as shown in Figure 2-4, the MPP actually changes with insolation, temperature and other conditions. Considering the high cost-per-watt of PV energy and the low conversion efficiency, it is crucial to extract as much power as possible to make it cost effective. Therefore the goal should be to make sure that the PV

14

panel operates at the MPP. This can be achieved by using power converters so that the PV panel always operates at the MPP. This technique is called maximum power point tracking (MPPT). A number of methods have been devised for MPPT some of which will be discussed next. Details about the power converters themselves will be discussed in Chapter 3.

2.3.2. PV Maximum Power Point Tracking Techniques

Numerous MPPT techniques have been reported in literature [11]. In general, most of these techniques can be categorized into four subgroups: Hill Climbing/Perturb and Observe method, Incremental Conductance method, Fractional Open-circuit voltage method and Fractional Short-circuit current method. It seems for that, among the four methods mentioned, there are subtle differences in the way they are implemented or in the control technique that is used. The general manner in which these methods work will be briefly discussed in the following sections.

Hill Climbing/Perturb and Observe Method

In this method, the duty cycle (the control variable) of a power converter connected to a PV array is periodically perturbed and the real-time power output of the PV array is measured. The power is measured at each sampling instant and it is then compared to the previously measured power. Figure 2-4(b) shows that when operating in the region to the left of the MPP, incrementing (decrementing) the voltage increments (decrements) power. If a perturbation of the duty cycle in a certain direction produces an increase in power, the subsequent perturbation should be kept in the same direction until maximum power is reached. Once this point is reached the system will operate at the MPP. The control algorithm is usually implemented using a microcontroller. The advantage of this method is

its ease of implementation and its ability to adapt to changes in insolation, temperature, and even changes in the PV array's own characteristics [12]. The drawbacks of this method include the possibility of settling at local maximum which may not necessarily correspond to the MPP, oscillations in the power output about the MPP, and slow response.

Incremental Conductance Method

Figure 2-4(b) shows that the slope of the PV power curve is positive to the left of MPP, zero at MPP and negative to the right of MPP. In effect, the following relations can be derived:

$$\frac{\Delta I}{\Delta V} = -\frac{I}{V}, at\ MPP$$

$$\frac{\Delta I}{\Delta V} = -\frac{I}{V}, below\ MPP \qquad (2.4)$$

$$\frac{\Delta I}{\Delta V} = -\frac{I}{V}, above\ MPP$$

The MPP can therefore be tracked by comparing the instantaneous conductance (I/V) to the incremental conductance ($\Delta I/\Delta V$). The main advantage of this method is that it is possible to track the MPP under rapidly changing atmospheric conditions and there is reduced oscillation in the power about the MPP [13]. The main disadvantage is that it requires a complex control circuit.

Open-Circuit Voltage Method

This method is based on the fact that there is a near-linear relationship between the PV array voltage at MPP, V_{MPP} and the PV array open circuit voltage, V_{OC}. This relationship is given by [13]:

$$k_v = \frac{V_{MPP}}{V_{OC}} \cong constant\ < 1. \qquad (2.5)$$

16

The proportionality constant, k_v, is roughly equal to 0.7 and it mainly depends on the solar cell fabrication technology and weather conditions. It has to be empirically determined before hand by measuring V_{MPP} and V_{OC} for a given PV panel at different levels of insolation and temperature. While tracking the MPP, the control algorithm momentarily shuts down the power converter every so often in order to measure V_{OC} and computes V_{MPP} using (2.5). The converter is then driven such that the PV array operates at this voltage. The main advantage of this method is that the control is very simple and consists merely of a voltage sensor and one feedback loop. The drawback of this method is that once k_v is chosen it is assumed constant even though changing characteristics of the PV panel and weather conditions might cause it to deviate from its initial value. Therefore, this method does not present a "true" MPP tracker. Another drawback is the fact that the panel has to be periodically open-circuited which leads a reduction in output power.

Short-Circuit Current Method

This method is based on the fact that there is a near-linear relationship between the PV array current at MPP, I_{MPP} and the PV array short circuit current, I_{SC}. This relationship is given by[13]:

$$k_i = \frac{I_{MPP}}{I_{SC}} \cong constant < 1. \tag{2.6}$$

The proportionality constant, k_i, is approximately equal to 0.9 and mainly depends on the solar cell fabrication technology and weather conditions. Measuring I_{SC} means additional switches might be required to short the PV panel thereby increasing the number of components and cost of the system. The method used in this work is an adapted version of the work done in [14]. In this work, the switch of a boost converter itself is used to short the PV array *and* is also used to directly control the PV current, resulting in a simpler

power circuit. The control is implemented using a digital signal controller. The details of implementation will be discussed in Chapter 4. The reasons and advantages of using this method in this work will be also become apparent in that chapter. The drawback of this system is that once k_i is chosen it remains fixed even though changing characteristics of the PV panel and weather conditions might cause k_i to deviate from its initial value. Therefore, this method does not present a "true" MPP tracker. Furthermore, the periodic shorting of the PV panels decreases the power output.

2.4. Conclusions

This chapter introduced various source of renewable energy and some of the key advantages of renewable energy were discussed. Since the work in this thesis involves wind and solar energy, these two sources were introduced in this chapter. Basic principles of wind energy conversion, including the types of wind turbines are discussed. This is followed by a discussion of the current WT technology. Wind turbine systems can be broadly classified as fixed-speed or variable-speed systems. Variable speed turbines are now the most common type of wind turbines which are normally connected to the grid via a power electronic system. Today the most commonly used variable speed WT configurations use a doubly fed induction generator (DFIG). Next, the characteristics of PV panels were discussed. Since maximum power has to be extracted from the panels, suitable MPP tracking techniques have to be implemented. A few of the more common MPPT methods were discussed and the advantages and disadvantages of each method were given.

CHAPTER 3. POWER CONVERTERS FOR WIND AND SOLAR ENERGY SYSTEMS

3.1. Introduction

The function of power electronics in renewable energy (RE) applications is to transfer power from the source to the load by converting voltages and currents from one form to another with the highest efficiency and lowest cost. Developments in power electronics have been instrumental in helping to improve the reliability of RE systems and have also helped to drive down costs. Among the various renewable components, wind turbine and PV systems extensively make use of power electronics. One issue with many power electronic converters is that they draw power from AC sources with highly distorted currents. This means that they operate at low power factors (PF) at the dismay of utility sources. This chapter first reviews the relationship between PF, distortion and total harmonic distortion (THD). Next, a review of various configurations of power converter systems used in wind energy systems particularly those utilizing DFIGs is presented. This is followed by a brief discussion about DC/DC converters used in PV applications.

3.2. Power Factor, Distortion, and THD

Utilities prefer that loads on their system operate at power factors close to unity. This is because loads that operate with low power factors draw power at higher values of root-mean-square (RMS) current. Many power electronic converters act as nonlinear loads which draw their power from the utility in the form of highly distorted currents which have a detrimental effect on the power quality of the utility source. Concerns about the effect of input current distortion on the power quality have led to the development of various

guidelines and standards intended to limit the amount of allowable distortion caused by power conversion systems. The amount of distortion in the current is quantified by the THD which is defined as [15]:

$$\%THD = 100 \times \frac{I_{distortion}}{I_{s1}} \qquad (3.1)$$

$$I_{distortion} = \sqrt{I_s^2 - I_{s1}^2}$$

where I_s is the RMS value of the distorted input current waveform and I_{s1} is the RMS value of the fundamental-frequency component of the input current. A high distortion in the input current leads to a low power factor. The power factor and the THD of the input current are related by the following expression [15]:

$$PF = \frac{1}{\sqrt{1+\left(\frac{\%THD}{100}\right)^2}} \cdot DPF \qquad (3.2)$$

$$DPF = \cos(\emptyset_1)$$

where DPF is the displacement power factor and $\emptyset_1$ is the angle by which I_{s1} lags behind the sinusoidal source voltage. From (2), we see that a high distortion (or %THD) in the input current, even at unity DPF, means a low PF. That is why utilities frown at systems or loads that draw highly distorted currents.

3.3. Power Converters for Wind Energy Systems with DFIGs

The electrical sub-systems of variable-speed wind energy systems tend to be more complex compared to those of fixed speed systems. In variable speed systems, a power converter usually connects either an induction or synchronous generator to the grid. The power electronic systems for variable speed systems must be able to adjust the frequency and voltage output of the generator to match that of the grid. This section introduces the

schemes that are typically used with variable speed wind energy systems utilizing DFIGs. Converter control is beyond the scope of this section and will not be discussed.

3.3.1. Static Kramer Drives and SCR converter

Figure 3-1 shows the schematic of a DFIG system utilizing a static Kramer Drive [16]. The converter consists of a passive three-phase diode-bridge rectifier on the rotor side and a line commutated inverter (SCR) on the grid side. Since the diode rectifier is unidirectional, power cannot be supplied to the rotor windings. Therefore, the static Kramer drive is only able to generate power when the DFIG is running at super-synchronous speeds in which case the power from both the rotor and the stator is supplied to the grid. In this system, the DFIG has to be magnetized from the stator which reduces its ability to provide reactive power control. In order to solve this problem, a second SCR converter is used on the grid side instead of the diode rectifier [17]. The system with the two back-to-back SCR converters is capable of producing more output power than the Kramer drive because reactive power can now be supplied via the rotor. The main disadvantages of this system are firing and commutation problems on the rotor-side converter and high harmonic distortion to the grid caused by the grid-side SCRs [18].
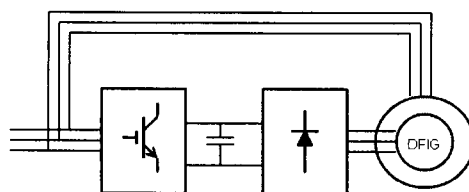
Figure 3-1: Static Kramer Drive

3.3.2. Vestas Converter System (VCRS)

Figure 3-2 shows the VCRS proposed by Vestas [19]. In this scheme the grid-side converter is a diode rectifier while the rotor side converter is a pulse width modulated voltage source inverters (PWM VSI). Therefore, the grid side converter is unidirectional while the rotor side converter is bidirectional. When the generator is operating below the synchronous speed, power flow is directed from the back-to-back converter stage and into the rotor. At speeds above the synchronous speed, the inverter is used in rectifier mode and the excess power from the generator is converted into a DC voltage for charging the DC link capacitor. To prevent an excessive rise in the DC link voltage, a power dissipating element is used to burn off the extra energy stored in the DC link. The advantage of this system is that the use of passive devices in the grid-side converter eliminates the need for complicated control circuitry and also increases the reliability of the converter since passive devices are more reliable than active components. However, a passive diode rectifier causes significant distortion in the input line current. Figure 3-3 shows the simulated waveform and the frequency spectrum of the input current drawn by a three-phase diode-bridge rectifier which show the high level of distortion. The total harmonic distortion (THD) of the waveform is almost 45%!

An alternative approach to using a diode rectifier for the grid-side converter is to use a power factor corrector (PFC) circuit. PFCs work by controlling the input current so that its waveform is always sinusoidal and in-phase with the mains voltage, i.e., the PF is made as close to unity as possible. PFCs can either be passive or active. Passive PFCs are basically filters which filter out the harmonics to improve power factor. However, the filters require

large sized inductors which are bulky and expensive. Furthermore, passive PFCs are not as effective as active PFCs.
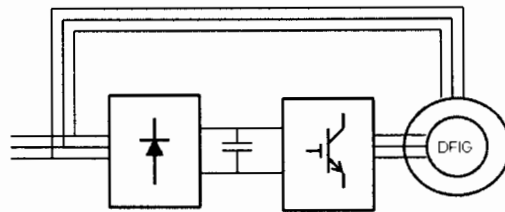
Figure 3-2: The Vestas VCRS Converter System

Several active power factor corrector (PFC) topologies and control methods for reducing the input current harmonics have been presented in recent years. Of these, the boost-type PFC topologies are more popular in applications since they show higher efficiencies [20]. Each of these topologies proposed have their pros and cons. For example, the three-phase PFC operating in continuous current mode (CCM) proposed in [21] has six switches, each of which is hard switched. Furthermore, it requires complicated control loops. A three-phase PFC with discontinuous current mode (DCM) [22] has just one active switch which makes the control loop design easier. However, it is difficult to drastically reduce the THD. In this project a resonant-boost three-phase PFC [20] is used for the grid side converter. This topology operates partly under DCM and partly under CCM, has a low input current THD, and has a high efficiency. Furthermore, no complicated control loops are required. More details about this circuit are presented in Chapter 4.
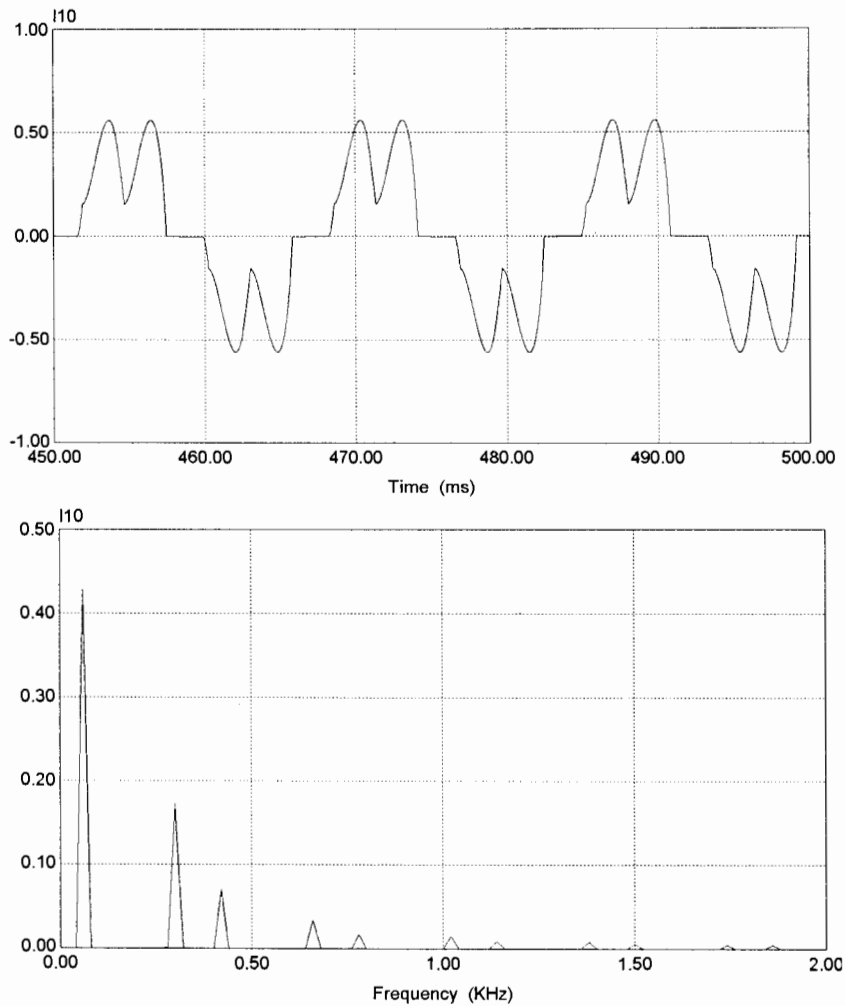
Figure 3-3: Diode-Bridge Rectifier Input Current Waveform with Waveform FFT

3.3.3. The Back-to-Back Two Level Voltage Source Converter

The back-to-back two-level voltage source converter shown Figure 3-4 is the most popular converter topology in wind turbine applications. This scheme consists of two converters which are connected back-to-back between the rotor and the grid. Both the converters are bidirectional PWM-VSIs and, together, they are capable of four quadrant operation. During sub-synchronous operation, the generator only supplies power to the grid via the stator and the grid supplies the rotor with injection power. Under this condition, the

24

grid-side converter acts as a rectifier and charges the DC link capacitor and the rotor side inverter injects AC power into the rotor windings of the DFIG. During super-synchronous operation, the rotor power is reversed and the generator supplies power to the grid through both the stator *and* the rotor. In this case, the rotor-side converter is operated in the rectifier mode feeding the DC link and the grid-side inverter supplies AC power to the grid. Both the converters are controlled independently of each other. The rotor side converter controls the active and reactive power by controlling the rotor current components. The grid-side converter controls the DC link voltage and ensures converter operation at unity power factor (i.e., zero reactive power).
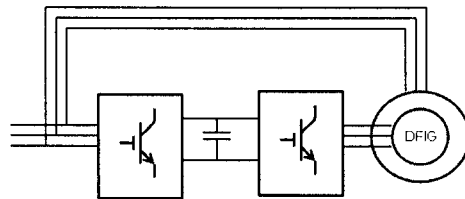
Figure 3-4: The Back-to-Back Two Level Voltage Source Converter

The scheme of Figure 3-4 has several advantages. The rating of the converters is selected based on the generator speed range and hence the slip power. It is typically only 25% of total system power with the generator speed range of ±33% around the synchronous speed [7]. Hence the cost of the converters is smaller compared to that of systems with full rated power converters. Active power and reactive power can both be independently controlled through the rotor excitation current. The magnetization current for the generator need not be provided only from the power grid through the stator but can

also be provided from the rotor circuit. The DFIG system is also capable of generating reactive power that can be delivered to the stator by the grid-side converter.

The main disadvantage of the back-to-back PWM-VSI are the high switching losses which can be attributed to fact that all the switches in both the grid-side and rotor-side converters are hard switched. With hard switching, there is a finite time when the switches have to withstand high voltage and high current at the same time and this translates to power loss and lower efficiency. Other problems associated with hard switching are device stresses, thermal management of power losses, and electromagnetic interference (EMI) due to high *di/dt* and *dv/dt* caused by fast transitions in the converter voltages and currents [15]. The fact that the back-to-back PWM-VSI system has two converters means that these problems are even more prominent.

3.4. DC/DC Power Converters for PV systems

DC/DC converters are widely used in photovoltaic generating systems as an interface between the photovoltaic panel and the load/energy storage unit. Depending on the type of application, DC/DC converters are capable of providing an average output voltage which is higher or lower than the input voltage supplied by the PV array. Changing insolation levels and PV operating temperatures means that the PV arrays typically have a wide voltage range. Therefore, the DC/DC converter also needs to have a wide input voltage range and at the same time regulate the output voltage. The power converters should also be highly efficient. An additional role of a DC–DC converter in the PV system is MPPT and the choice of the DC/DC converter has an impact on the MPP-tracking efficiency [23]. The three most commonly used converter topologies are the Buck, Boost

and Buck–Boost converters. Each of these will be briefly discussed in the following sections.

3.4.1. Buck Converter

In a Buck converter (Figure 3-5), the average output voltage is less than the input voltage. The steady state average output voltage V_O is given by:

$$V_O = DV_{in} \qquad (3.3)$$

where V_{in} is the input voltage (supplied by the PV array) and D is the duty cycle. The buck converter requires just a single switch which makes it very efficient. The downside to this converter is that the input current is likely to be discontinuous and a fairly large smoothing input capacitor (C_1) is normally required.
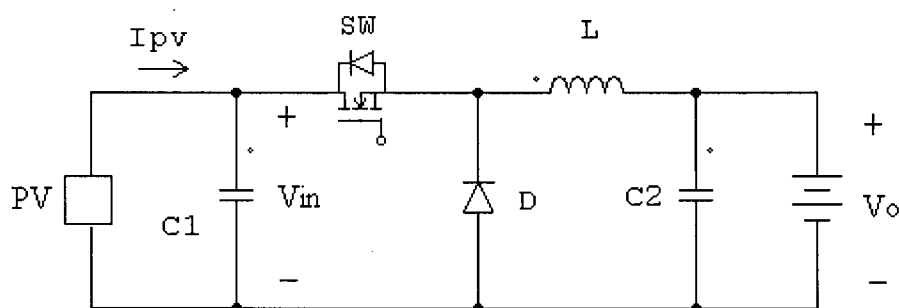
Figure 3-5: Buck Converter

3.4.2. Boost Converter

In a boost converter (Figure 3-6), the output voltage is always greater than the input voltage. The steady state output voltage of the boost converter in the continuous current mode (CCM) is given by:

$$V_O = \frac{1}{1-D}V_{in}. \qquad (3.4)$$

The converter requires just one switch and is therefore highly efficient. The input current is normally continuous which means that a boost converter needs a smaller input

filter capacitor than a buck converter. The downside to this converter is that a high peak current flows through the power transistor. Furthermore, the boost converter requires a larger inductor (L) and an output filter capacitor (C_2) than the buck converter. This is because the average output current is (1-D) times lower than the inductor current and a higher RMS current flows through the capacitor. Additionally, the output voltage is very sensitive to changes in D and this can result in stability problems during closed loop operation.
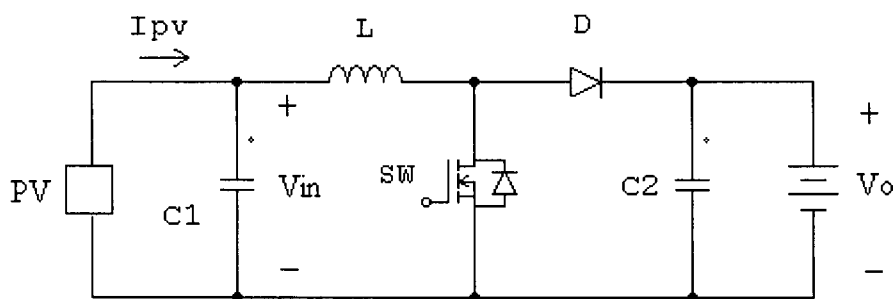
Figure 3-6: Boost Converter

3.4.3. Buck-Boost Converter

In Buck-boost converters (Figure 3-7), the output voltage is allowed to be either greater or lower than the input voltage depending on D. The steady state output voltage of the buck-boost converter in the continuous current mode (CCM) is given by:

$$V_O = \frac{-D}{1-D} V_{in}$$
(3.5)

and the polarity of V_o is opposite to that of V_{in}. A buck-boost converter also uses just one switch and so has a high efficiency. The downside is a discontinuous input current and a high peak current flowing through the transistor.
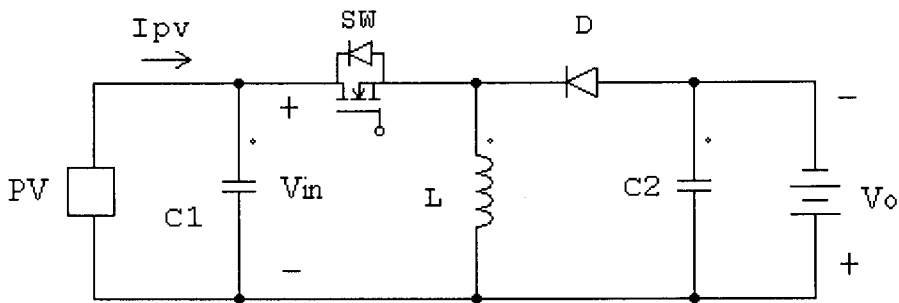
Figure 3-7: Buck-Boost Converter

There following are two variations of the buck-boost topology:

1) SEPIC converters – these are used in applications where the input current is continuous. Unlike the buck-boost converter, the SEPIC converter has an output voltage whose polarity is that same as that of the input voltage.

2) Cuk Converters – unlike the buck-boost converter, the Cuk converter has a non-pulsating current at both the input and the output. The output voltage polarity is opposite to the input polarity just like the buck-boost converter.

3.4.4. Topology Selection

The voltage/current stress experienced by the switches and diodes in the three converter topologies are compared in Table 3-1 [15]. The stresses listed are under the assumption that the ripple current in the inductor is negligible. Table 3-1 can be used as a guideline to determine which converter topology is best suited for a particular application. Table 3-1 shows that the buck-boost converter sees much higher currents and voltages than either the buck or the boost converter which means its components are subject to higher stresses. Furthermore, it suffers from pulsations in both the input and output currents. Since the input current is supplied by the PV array, a pulsating current in the PV output can make it difficult to track the MPP. The buck-boost converter should therefore be used only if

29

both buck and boost capability is needed. Otherwise, the buck or the boost converter should be used based on the desired capability. One caveat is that the buck converter also suffers from a discontinuous input current. Care must therefore be taken to make sure that an appropriately sized input filter capacitor is used.

In grid tied applications, for example, the PV arrays are connected to the grid via two power converter stages: a DC/DC converter and then a DC/AC inverter. PV arrays typically output low DC voltages. The input voltage of the inverter, however, must be raised to a voltage higher than the grid voltage, so generally a boost DC/DC converter is used. There is also an additional advantage in using a boost converter in PV applications. During night time, when the PV cells do not produce any voltage, power could flow back into the PV cells and cause damage. The boost configuration has series diode that can act as a blocking diode and so a separate diode is not required to protect the PV panels.

Table 3-1: Topology Selection Criteria

Device	Variable	Buck	Boost	Buck-Boost
Transistor	V_{peak}	V_{in}	V_o	$(V_{in} + V_o)$
	I_{peak}	I_o	I_{in}	$I_{in} + I_o$
	I_{rms}	DI_o	DI_{in}	$D(I_{in} + I_o)$
	I_{av}	DI_o	DI_{in}	$D(I_{in} + I_o)$
Diode	I_{av}	$(1-D)I_o$	$(1-D)I_{in}$	$(1-D)(I_{in}+ I_o)$
Load	I_L	I_o	I_{in}	$I_{in} + I_o$

3.5. Conclusions

Power electronic converters are widely used for RE systems as power conditioning systems and MPPT. The issue with most power electronic converters is that they act as nonlinear loads drawing highly distorted currents with high THD values. This chapter first

reviewed the relationship between PF, distortion and total harmonic distortion (THD). Next, a review of various configurations of power converter systems used in wind energy systems utilizing DFIGs was presented. This is followed by a brief discussion about DC/DC converters used in PV applications.

CHAPTER 4. HYBRID RENEWABLE ENERGY SYSTEM WITH WIND TURBINE AND PV PANELS

4.1. Introduction

Renewable energy sources like wind energy and photovoltaic (PV) power are becoming popular. Doubly fed induction generators (DFIGs) are increasingly used in wind generating systems in which the rotor speed need not be maintained constant. These systems use a wound-rotor induction machine to convert the mechanical power from the wind turbine into a fixed-frequency AC output supplied to the grid. The frequency of the voltage injected into the rotor is adjusted such that the sum of rotor frequency and the equivalent frequency corresponding to mechanical rotation is equal to the desired stator frequency (60Hz). In this scheme, the power required for rotor injection is a small fraction (25%) of the output power and it comes from the AC mains through a set of power converters [22], [24]. Thus the system uses power converters as well as filters with correspondingly lower ratings. The inverter provides a three-phase sinusoidal voltage to the rotor terminals at a frequency determined by the mechanical speed of the rotor. The DC link voltage for the inverter is usually provided by a converter/rectifier.

Some of the issues not addressed by the existing DFIG control schemes are: (a) the absence of power factor correction in the rectifier (b) the absence of soft switching that could improve the efficiency of the rectifier and (c) the ability to supply AC power to isolated loads using photovoltaic power. As for (c), PV panels installed alongside the wind turbine can be used to aid wind generation particularly when the system uses a DFIG.

This chapter presents a *hybrid* scheme in which the injection power can be drawn from (a) AC mains at unity power factor if available or (b) a set of PV panels and a back-up battery in the absence of AC mains. The three-phase power from the AC mains is converted into a DC using a three-phase resonant-boost power factor corrector (PFC) with only two switches implementing zero voltage switching (ZVS) [20]. In the absence of the AC bus, a set of PV panels supply injection power to the rotor through a boost converter which is realized using one or more of the switches in the power factor corrector. A current-based MPP tracking system is implemented to ensure that maximum power is extracted from the PV panels. A battery can be added as (a) a buffer storing the extra energy from the PV panel when the maximum power available is more than what is required for rotor injection and (b) a DC source providing injection power in the absence of sun light. A three-phase Sine PWM inverter is used to convert the DC voltage from the three-phase PFC/ PV converter and provide the rotor injection voltage to the DFIG. A Sine PWM based slip control scheme together with constant volts/hertz control is implemented for the rotor-side converter to ensure that the magnitude and frequency of the stator voltage of the DFIG are maintained constant.

Normal operation for the DFIG for the proposed system is at sub-synchronous speed where the inverter injects power into the rotor. However, above the synchronous speed, the rotor power flow is reversed. In this case the inverter can be used as a rectifier and the excess power from the DFIG rotor could be used to charge a battery connected across the DC link. However, this might require an additional DC/DC converter if the battery voltage is higher/ lower than the DC link voltage. It is to be noted that the PFC is

unidirectional and will prevent the power from being returned to the grid. Experimental and simulation results for the various segments of the hybrid system are presented.

4.2. Three Phase Power Factor Corrector

The power converter system proposed for rotor injection in a DFIG is shown in Figure 4-1. The three-phase PFC is made up of the line inductors L_a, L_b, L_c, the diodes D_1-D_8, the resonant capacitors C_a, C_b, C_c, the resonant inductor L, and the MOSFETS M_x and M_y [20]. The PFC draws sinusoidal currents from the bus (V_a, V_b, V_c) and supplies a DC voltage to the three-phase inverter which in turn supplies a variable-frequency three-phase sine voltage to the rotor of the DFIG. The three-phase inverter is a Sine PWM inverter and its output frequency and voltage magnitude are varied through feedback to have the DFIG supply rated stator voltage at 60Hz.
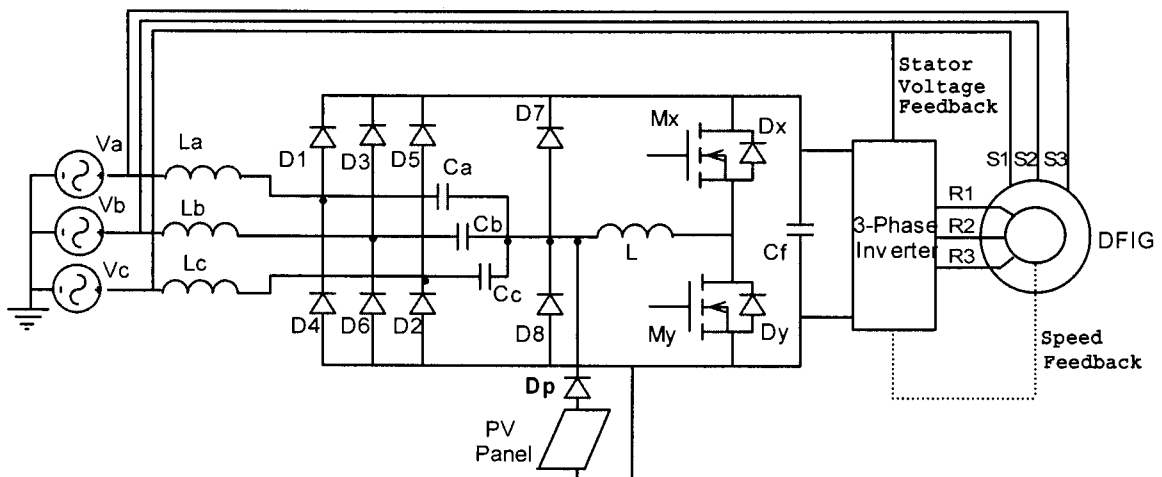
Figure 4-1: Power Converter Arrangement for a DFIG

DFIG systems with a static Kramer drive utilize a line commutated inverter connected to the supply side [16]. The major drawback of this approach is high harmonic

distortion in the current fed to the grid caused by the supply-side thyristor converter [18]. In DFIG systems utilizing back-to-back converters, the three phase voltage from the AC mains is rectified with a PWM switch-mode three-phase voltage-source-inverter (VSI) operating in rectifier mode. PWM techniques could be used to actively shape the input current drawn from the grid close to a sinusoid thereby reducing harmonics. However, this would require complicated current control loops. Furthermore, the active switching of six switches in the converter can typically lead to undesirable power losses during power conversion. The VCRS scheme proposed by Vestas [25] uses a passive grid-side diode rectifier. Using passive devices in the converter eliminates the need for complicated control circuitry and also increases the reliability of the converter since passive devices are more reliable than active components. However, a passive diode rectifier causes significant input line current harmonic distortion. The key advantages of using the proposed PFC are unity input power factor and significantly reduced input line current harmonic distortion. The PFC circuit only uses two switches which helps to minimize power losses and gives excellent efficiency. Using fewer active components also helps to make the converter more reliable. Furthermore, the circuit automatically shapes the input current which eliminates the need for complex current control loops.

In typical DFIG schemes utilizing back-to-back converters, the three phase voltage from the AC mains is rectified with a PWM switch-mode converter in which the switches are required to turn on and turn off the entire load current each time they switch. This is referred to as hard switching. During the turn on and turn off process, the hard switched devices have to momentarily withstand high voltage and high current simultaneously and are subjected to high switching stresses and a high switching power loss which increases

linearly with switching frequency. Another significant problem with switch mode operation is the electromagnetic interference (EMI) caused by the high value of the voltage derivative with time *(dv/dt)*. The PFC operates under ZVS condition which means that the voltage across each switch goes to zero before it turns on and allows the current to flow. Therefore, the power dissipation that would normally occur during switching transitions is eliminated leading to a highly efficient converter ($\approx$ 98%) while reducing the radio frequency (RF) noise considerably.

In the PFC topology, three capacitors are used to decouple the three-phase system into three single-phase systems and to control each phase independently and this helps to obtain a low THD value for each input current while delivering a lower output DC voltage. The section with the two switches M_x and M_y and the inductor L constitutes a high-frequency current source which is responsible for the energy transfer from the three phase AC side to the DC side. Both the power switches turn on and off under zero-voltage-switching (ZVS) condition. The input current is partly continuous and partly discontinuous depending upon the input voltage level which modulates the equivalent duty cycle for the inductor current.

For a balanced three-phase system, the converter can be decoupled into three single-phase PFC converters and analyzed [20]. The input capacitor C_a first transfers part of the input energy to the inductor L and the energy is then transferred to the DC filter capacitor and the load while maintaining a constant output voltage V_{DC}. Depending on the magnitude of the instantaneous input voltage, the circuit may operate under (i) a resonant input mode or (ii) a boost input mode. The resonant input mode corresponds to a low instantaneous input voltage, and during this mode, the voltage on C_a is less than V_{DC}. The

36

boost input mode, on the other hand, corresponds to a high instantaneous input voltage, and during this mode the voltage on C_a is slightly less than V_{DC}.

The input/output power can be controlled by controlling the amplitude of the high-frequency current source which is in turn controlled by the switching frequency. The following equations are used to design the converter [20]:

$$\frac{1}{2*f_{sw}} = \pi * \sqrt{LC_a} + L * \frac{I_m}{V_{dc}} \tag{4.1}$$

$$P_{in} = K\sqrt{\frac{C_a}{L}} \tag{4.2}$$

where f_{sw} is the switching frequency, I_m is the amplitude of the current through the resonant inductor and K is a proportionality constant. The output DC voltage is approximately equal to $\sqrt{2}V_{LL}$ where V_{LL} is input line-to-line voltage.

The three-phase PFC was designed for operation at an input voltage of 120Vline-to-line at 60Hz and an output power of 300W at about 200V_{DC}. The switching frequency (f_{sw}) of the MOSFETs was selected as 155 kHz which was found through simulation to give low distortion in the input current. The values of the components, $L_a = L_b = L_c$, and $C_a = C_b = C_c$, and L for the PFC are found through simulation for supplying a nominal power to the rotor of the DFIG. The PFC circuit was simulated using the software PSIM [26] which provides a powerful simulation environment for power electronics and motor control. The waveform of input current and its frequency spectrum are obtained. The harmonic amplitudes in the input current and the total harmonic distortion (THD) for different input voltages were obtained to show the effectiveness of the circuit in handling a wide range of input voltages.

4.2.1. Simulation Results

The PFC circuit was simulated for two values of input voltage, and the simulation parameters and results are summarized in Table 4-1. The output of the PFC was connected across a resistive load, R. An input voltage of 120Vline-line provides an output voltage close to the desired DC output voltage of 200V. It is seen that the THD is less than 10% and the converter efficiency is very high. The waveform of one of the line currents and its frequency spectrum obtained from the simulation of the PFC circuit are shown in Figure 4-2 and Figure 4-3 respectively. The input current is sinusoidal and is perfectly in phase with the input voltage which means a unity PF. It contains the 5th and 7th harmonics which are the only significant lower order harmonics. Table 4-1 gives the output DC voltage and THD for a range of input voltages and it is seen that the three-phase PFC has a consistently low distortion over a range of input voltages. The input current THD is calculated using:

$$THD, \% = \sqrt{\frac{\sum_{k=5}^{\infty} I_k^2}{I_1^2}} * 100 \tag{4.3}$$

where I_1 is the RMS value of the fundamental component and I_k is that of the kth harmonic.

Table 4-1: PSIM PFC Simulation Results

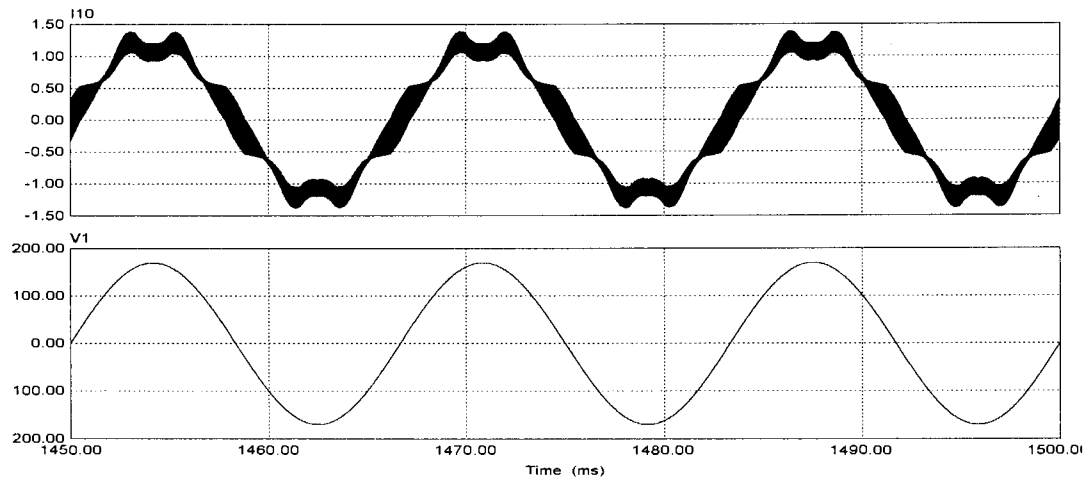| V_{in} (VLL)	f_s (kHz)	C_a, C_b, C_c (nF)	L_a, L_b, L_c (mH)	L (uH)	R (ohm)	V_{out} VDC	P_{in} (Watts)	P_{out} (Watts)	Eff. (%)	THD (%)
120	155	5.1	0.4	65	300	172	102	99.8	97.8	9.25
208	155	5.1	0.4	65	300	300	306	296	96.7	9.25

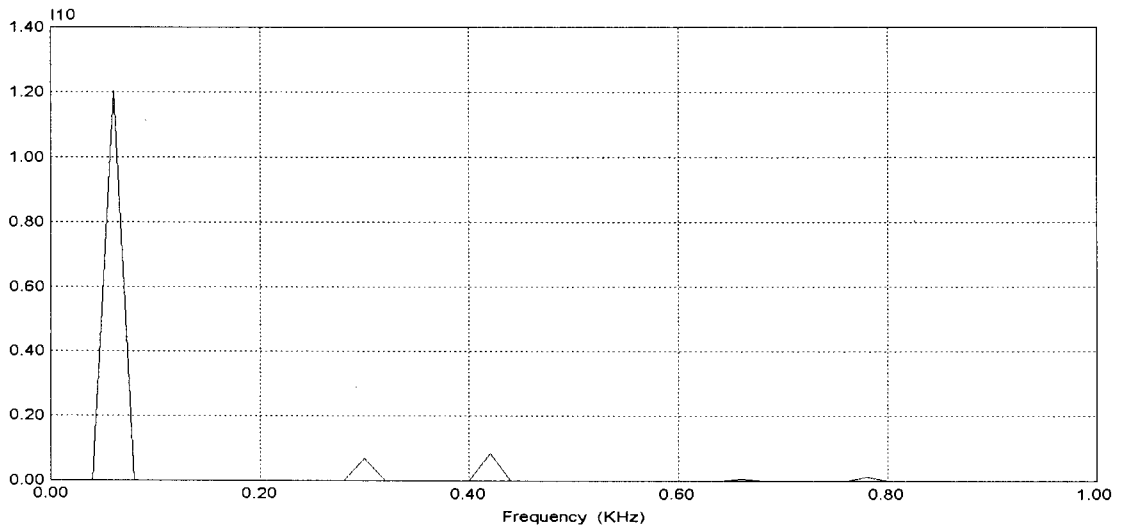*Figure 4-2: Simulated Waveforms of Line Current and Voltage*

Figure 4-3: Line Current Frequency Spectrum from Simulation

Table 4-2: Variation of Output Voltage and THD with Input Voltage
($f_s = 155$ kHz, $R = 300\Omega$)

V_{in}, Volts	52	104	166	208
V_{DC}, Volts	74.4	148.8	237.5	297.6
THD, %	9.25	9.25	9.25	9.25

39

4.2.2. Experimental Results

The three-phase PFC was built and tested. The component values were the same as the ones used for simulation. The switches are N-channel MOSFETs and the diodes are ultrafast diodes. The 155 kHz gate pulses were provided to the circuit utilizing a TL494 PWM control integrated circuit (IC). The gate pulses can also be easily provided by a DSC. The experimental waveform of one of the line currents and its frequency spectrum are shown in Figure 4-4. The THD is found to be 8.1% which is very close to the result obtained by simulation. The output DC voltage is 169.8V for a three-phase input voltage of 120V line. The waveforms of the gate signal to M_y and the drain-source voltage of M_y are shown in Figure 4-5 and it is seen that the drain-source voltage (V_{ds}) goes to zero before its gate pulse (V_{gs}) is applied showing zero voltage switching condition.

4.3. PV Power and Maximum Power Point Tracking

During grid-connected operation, the three-phase PFC supplies DC power to the inverter which in turn provides a variable-frequency AC voltage to the rotor of the DFIG. For isolated loads, the injection power is drawn from the PV panel through a boost converter made up of the high-frequency inductor L, the MOSFET M_y, and the diode D_x which are part of the three-phase PFC shown in Figure 4-1. The obvious advantage of not requiring a separate DC-DC converter for the PV panel should be noted. In this case, the bulk capacitor C_f is replaced by a battery which provides injection power in the absence of sunlight. During night or in the absence of sunlight, the battery may be charged by rectifying the 3-phase AC voltage output of the DFIG. The duty cycle of M_y is adjusted for extracting the maximum power available from the PV panels under a given level of insolation.
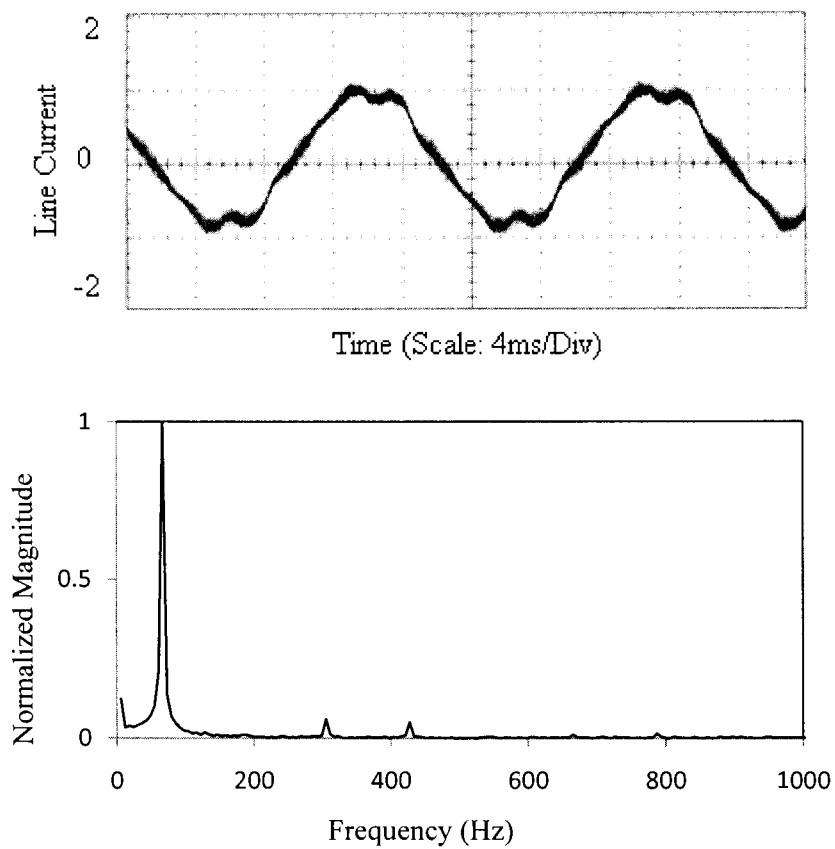
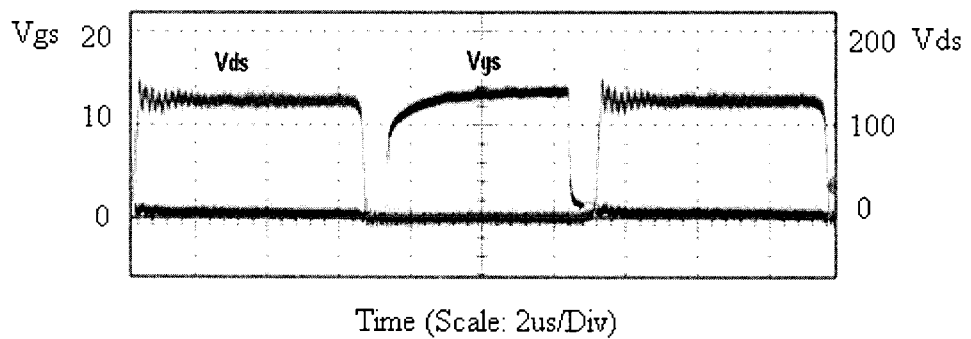*Figure 4-4: Experimental Waveforms of Line Current and Frequency Spectrum*

Figure 4-5: Experimental Waveforms of Drain and Gate Voltages

41

If the power output from the PV panel exceeds the power required for rotor injection, then the excess power goes to charge the battery. Otherwise the battery supplies the difference. The voltage rating of the PV panels and the number of panels are selected such that it possible to boost the panel output to the rated DC link voltage of the inverter with reasonable values for the duty cycle.

Four 120W PV panels (Solarex SX-120) connected in series give a maximum output of 400W at a voltage of 120V under medium sunlight conditions. With this, it is possible to step up to 200V matching the output from the 3-phase PFC. If the DFIG speed is limited to slip value ± 0.25, with a PV power of 400 W available for rotor injection, the wind generation scheme can output a power as high as 1500W.

4.3.1. Maximum Power Point Control of Boost DC-DC Converter

In order to extract the maximum amount of power from the PV panel, the converter must be operated to keep the PV panel at its MPP at all times. In this work, the PV system employs a current-based maximum power point tracking (MPPT) scheme which uses the fact that the PV current at MPP is linearly related to the short-circuit current [27], [28]. This relationship is given by:

$$k_i = \frac{I_{MPP}}{I_{SC}} \cong constant < 1. \tag{4.4}$$

The proportionality constant k_i is approximately equal to 0.9 and it mainly depends on the solar cell fabrication technology and weather conditions. Measuring I_{SC} means additional switches might be required to short the PV panel thereby increasing the number of components and cost of the system. The method used in this work is an adapted version of the work done in [14]. In this work, the switch of a boost converter itself is used to short the PV array *and* is also used to directly control the PV output current, resulting in a

42

simpler power circuit. The generalized power circuit and control circuit are shown in Figure 4-6. The complete MPPT including the proportional plus integral (PI) controller is realized using a Digital Signal Controller (DSC) from Microchip (dsPIC30f2020) [29]. A PWM generator within the Motor Control PWM (MCPWM) module on the DSC device supplies the gate signals. In order to track the MPP, the PI controller forces the PV current to be a fraction (0.9) of the short circuit current by adjusting the duty cycle of M_y.

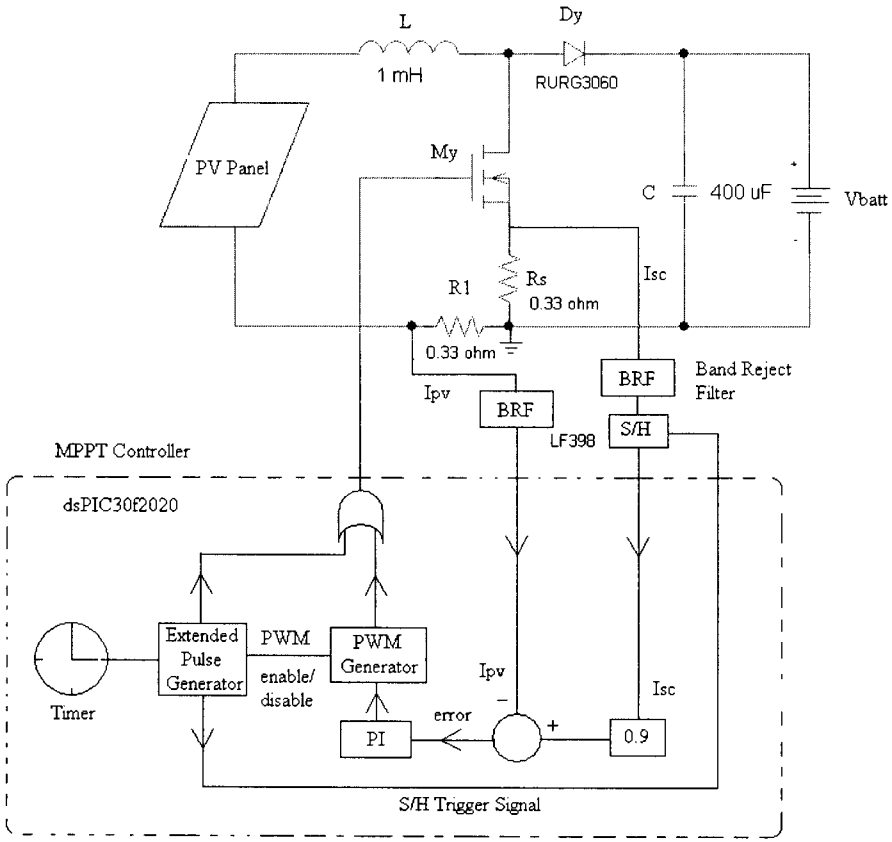

Figure 4-6: Block Diagram of MPPT Converter

The scheme senses the short circuit current under a given insolation by applying a long pulse to M_y which shorts the PV panel. The voltage sensed across the sensing resistor

R_s is applied to a sample-and-hold (S/H) IC which provides the short circuit current (I_{sc}) data to the DSC. A band reject filtering stage is used to filter out the noise in the 60 – 120 Hz range. The trigger signals for the S/H IC is provided by the DSC. The extended pulses applied to the switch M_y are applied once in several switching cycles. Figure 4-7 shows illustrative waveforms of the whole process. Periodic gate pulses of the required duty cycle provide the necessary boost ratio. After several switching cycles, these periodic pulses are interrupted with an extended pulse (Figure 4-7 (a)). At this time the DSC also sends a trigger signal to the S/H IC to start sampling (Figure 4-7 (d)). Figure 4-7 (b) shows that the short circuit current has some transient behavior. This is because the short circuit current has to flow through the inductor. Therefore, it is necessary to make sure that the extended pulse is sufficiently long enough to allow the current to reach the steady state value. Once the short circuit current (I_{sc}) reaches its steady state value, another signal is sent by the DSC to instruct the S/H IC to hold that value. The output of the S/H IC (Figure 4-7 (d)) will now represent the new value of I_{sc} and will serve as the reference signal for the PI controller.

The actual PV current, I_{PV}, is needed at every switching cycle and is obtained by measuring the voltage across the sense resistor R_1 and this information is also provided to the DSC via a filtering stage. The illustrative waveform of I_{pv} is shown in Figure 4-8. A PWM trigger functionality of the DSC is employed to trigger the Analog-to- Digital Converter (ADC) module on the DSC so that I_{PV} is always sampled at half ton, where t_{on} is the on-time of the switch. This ensures that the average value of I_{pv} is obtained each time.

4.3.2. DSC Implementation

Figure 4-6 shows a block diagram of the DSC-control circuit. The voltage signals representing I_{PV} is routed through the filtering and gain stages and fed directly to an input

pin of the ADC module. The signal representing I_{SC}, on the other hand, is first passed through the sample-and-hold IC (LF398) so that a continuous waveform representing I_{SC} (like Figure 4-7(c)) can be obtained. Figure 4-9 shows the connections for the S/H IC LF398. The value of C_h is selected to be 0.01μF which will ensure an acquisition time of less than 10μs. The S/H trigger signal (logic signal) is supplied from one of the general purpose input-output (GPIO) pins of the dsPIC.

The 10-bit ADC module on the DSC has a reference voltage of 5V which means it is capable of a resolution of 4.88mV per bit. It is also capable of completing the 10 bit conversions in 1μs. The ADC is configured to trigger the conversion of the I_{PV} signal using a trigger from the PWM module as described earlier. This guarantees an accurate measurement of the average current at every switching cycle (50 kHz). The conversion of the I_{SC} signal is driven by a general purpose timer (Timer1) interrupt that also controls the instant when the extended pulse to the switch is applied. The timer interrupt is configured so that the PV panel is shorted and the ADC module converts the I_{SC} signal once every 20ms. The PWM generator is configured to provide a switching frequency of 50 kHz and to allow the PWM duty cycle to be changed on-the-fly.

DSC Source Code

All the programming for the DSC was developed in C language in the MPLAB IDE and the code files used and a brief description of each are provided in Table 4-3. Hex files created were downloaded to the DSC via the PICkit2 Programmer software. Figure 4-10 shows the flow chart for the PV MPPT control routine. The interrupt routine of Timer1 sets the PI Flag at a frequency of 50 Hz (period = 20 ms). When the PI Flag is set, the program initiates the main routine to apply an extended pulse, measure I_{SC}, calculate the error (=

0.9*I_{SC} – I_{PV}), and run through the PI routine. The ADC interrupt routine is set to measure I_{PV} at every switching cycle.
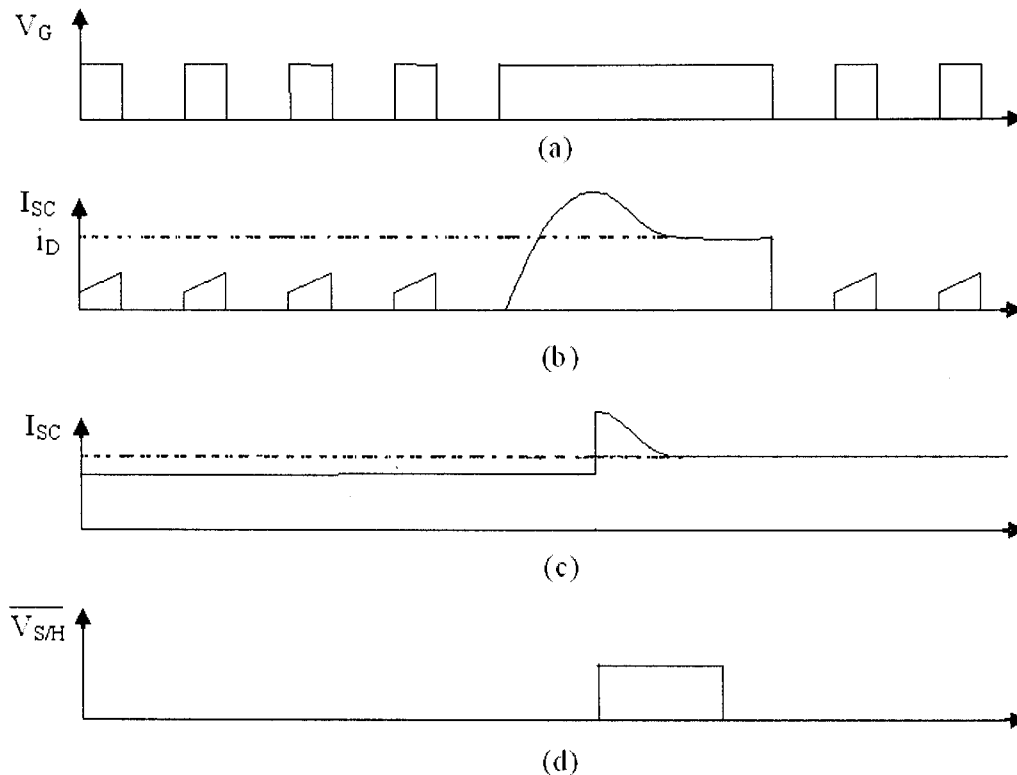

Figure 4-7: Illustrative Waveforms of MPPT Controller: (a) Gate Signals to M_y, (b) Current flowing through R_s, (c) I_{SC} output from S/H IC, (d) Trigger Signals to S/H Circuit from the DSC.
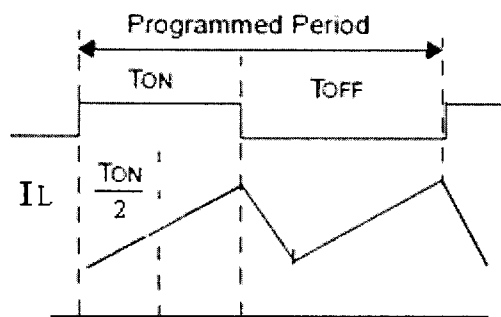

Figure 4-8: I_{PV} Waveform and Sampling
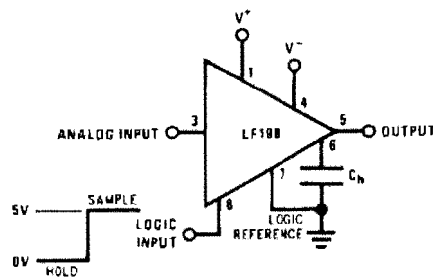
Figure 4-9: LF398 Sample-and-Hold IC

The flowchart for the PI routine is shown separately in Figure 4-10. To obtain the integral term, the accumulated error must first be determined and it is simply the sum of the past errors. Accumulative error limits are introduced to prevent integral wind-up which occurs when the accumulative error keeps increasing and the plant output is saturated. The constants K_p and K_i represent the proportional gain and the integral gain respectively. PDC is the register which holds the duty cycle information for the PWM Generator, and the duty cycle can be changed with a resolution of 0.0078%. The variables PDC_{MIN} and PDC_{MAX} represent the minimum and maximum allowable values of duty cycle and these are chosen to be 5% and 95%.

Table 4-3: Description of DSC Code Files

File name	Type	Description
boost code.c	Source File	Main software routine
Function.c	Source File	Source code for routinely used operations
math.h	Header File	Header file for basic mathematical operations
p30F2020.h	Header file	DSPIC header file
p30f2020.gld	linker script	DSPIC linker script

4.3.3. Extended Gate Pulse Generation

As motioned earlier, the short circuit current I_{SC} is measured by shorting the PV panels by applying an extended gate pulse and then waiting for I_{SC} to reach steady state

value before it could be sampled. This means is that there is a minimum time delay, t_{Dmin}, between the rising edge of the extended pulse and the instant I_{SC} is sampled by the S/H IC. Therefore, in order to ensure proper operation, the extended pulse period must exceed t_{Dmin}. The time constant for power converter during the short-circuit process can be easily determined by considering an equivalent R-L circuit consisting of the inductor, the two sense resistors R_{SH} and R_S, and the $R_{DS(ON)}$ value of the MOSFET. The current is then given by:

$$I_{SC} = \frac{V_O}{R_{eq}}(1 - e^{-R_{eq}*t_{D}/L}), \tag{4.5}$$

and

$$R_{eq} = R_S + R_{SH} + R_{DS}$$

where V_O is the output voltage of the boost converter, L is the value of the inductor and R_{eq} is the equivalent resistor of the circuit when the switch is turned on. An expression for t_D can be easily derived from (4.5) as:

$$t_D = -\frac{L*ln\left(1-\frac{I_{SC}*R_{eq}}{V_O}\right)}{R_{eq}} \tag{4.6}$$

Using L = 1mH, $R_{SH} = R_S = 0.33\Omega$, $R_{DS(ON)} = 0.11$, $V_O = 200V$ and $I_{SC} = 2.7A$ in (4.6), t_{Dmin} is found to be approximately 13.6µs. The duration of the extended gate pulse should therefore exceed 13.6 µs in order to ensure I_{SC} has reached its steady state value.

4.3.4. Filter Design

The input signals representing I_{SC} and I_{PV} are the voltages across the two sense resistors as shown in Figure 4-12. A band reject filter is designed to prevent the noise in the 60 – 120 Hz range from being coupled on to the signal. It utilizes low noise, precision

operational amplifiers. The gain is adjusted so that the output does not exceed the maximum input voltage of 5V for the ADC within the DSC.

4.3.5. Inductor Selection

As shown in Figure 4-6, one of the inputs to the PI controller is the actual PV current I_{PV}. The boost converter is designed to operate in the continuous current mode (CCM) so as to minimize the PV ripple current. In order to ensure operation in the CCM, the inductor should have a minimum value given by [30]:

$$L_{min} = \frac{T_S V_o}{2 I_{OB}} D(1 - D)^2 \tag{4.7}$$

where T_s, V_O, I_{OB} and D are respectively, the switching period, output voltage, average output current and duty cycle (DC). For a worst case design, V_O is chosen to be 200V. For a switching frequency of 50 kHz, T_s is 20 μs. The nominal duty cycle is expected to be in the range $0.3 - 0.9$ and so the lowest duty cycle is chosen to be 0.3. Since the converter output current will be driven to 0.9 times the PV panel short circuit current ($\approx$1A), I_{OB} is taken to be 0.9A. The use of these values in (4.7) gives L_{min} to be 0.33mH. An inductor value of 1mH was chosen for this part of the project to ensure CCM operation.

4.3.6. Experimental Waveforms

The PV MPPT controller was first tested using a solar lamp station consisting of four 1000 Watt Metal Halide lamps that produce light in most regions of the spectrum and a PV panel with a maximum power output of about 10W. Figure 4-13 shows the waveforms of the inductor current, the output of the S/H IC and the PWM gate signals to the switch. The switch gate signal waveform shows the high frequency PWM signals of a specific duty cycle as well as the extended pulse for sensing I_{SC}. The inductor current

49
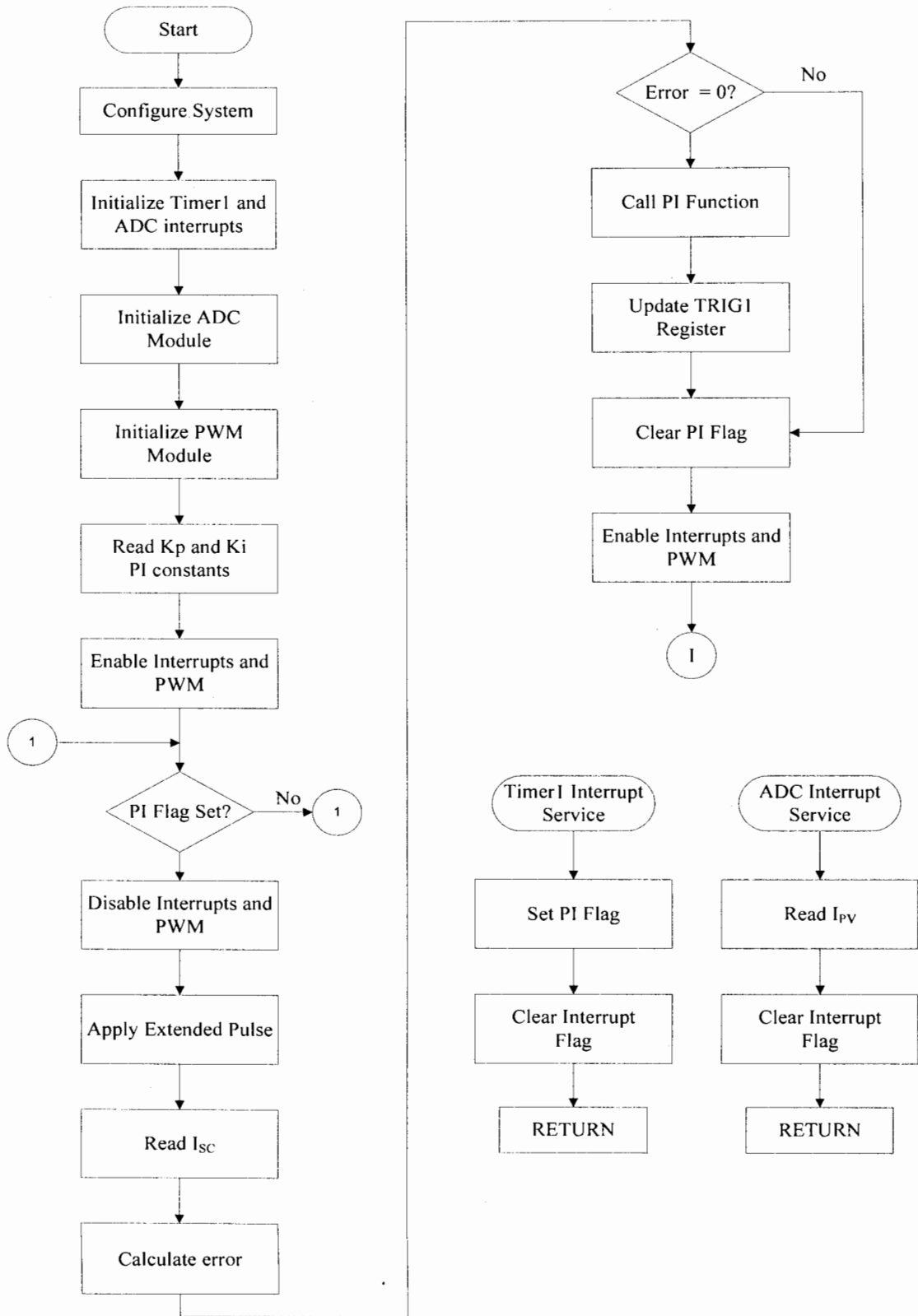
Figure 4-10: PV MPPT Controller Routine Flow Chart

50
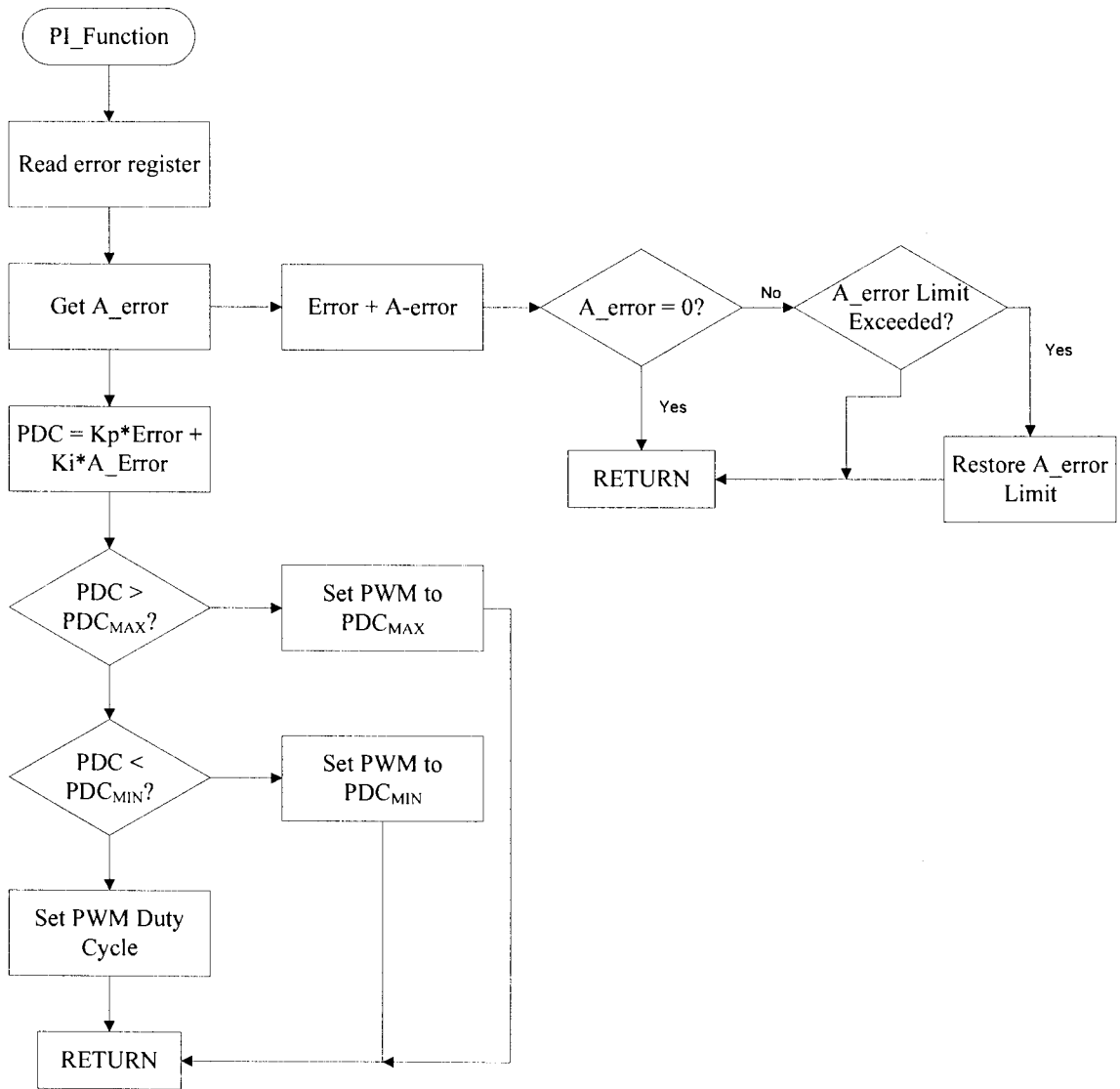
Figure 4-11: PI Routine Flow Chart
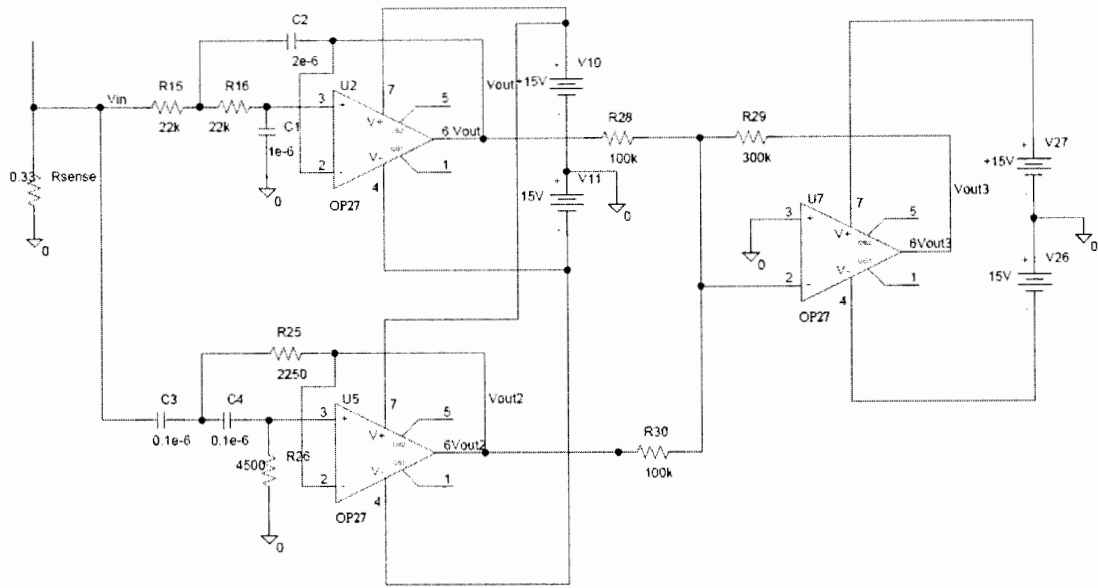
Figure 4-12: Band Reject Filter

waveform shows the transient portion of the short circuit current which starts at the rising edge of the extended pulse. By the time the extended pulse is removed, I_{SC} has reached its steady state value.

Figure 4-14 shows I_{PV} tracking I_{SC} over a period of ten seconds. A step in insolation is applied by turning two of the four lamps off. It is seen that the tracking algorithm works quite well. The controller was also tested to see if the PV panel delivered the respective maximum powers for different loads. The resistive load on the boost converter was varied from 40Ω to 155Ω and the power was measured. Figure 4-15 shows that the power output from the PV panel stays fairly constant at about 10W for different loads thus confirming the MPPT.

52
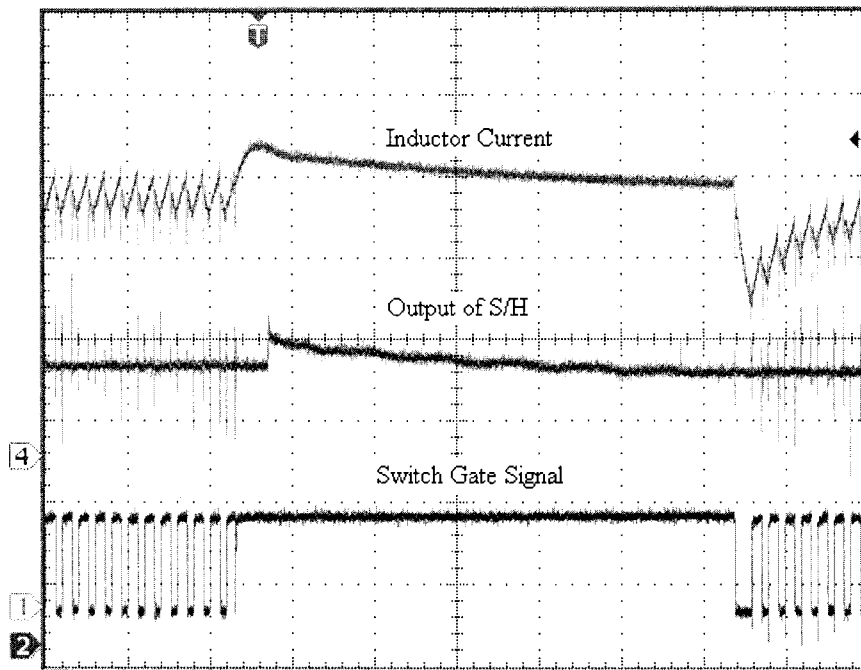
Time Scale: 50µs/Div; Vertical Scale: (1) Inductor current: 1V/Div, (2) S/H output: 1V/Div, (4) Gate signal 10V/Div

Figure 4-13: Experimental Waveforms of Inductor Current, Output of S/H and Switch Gate Signals
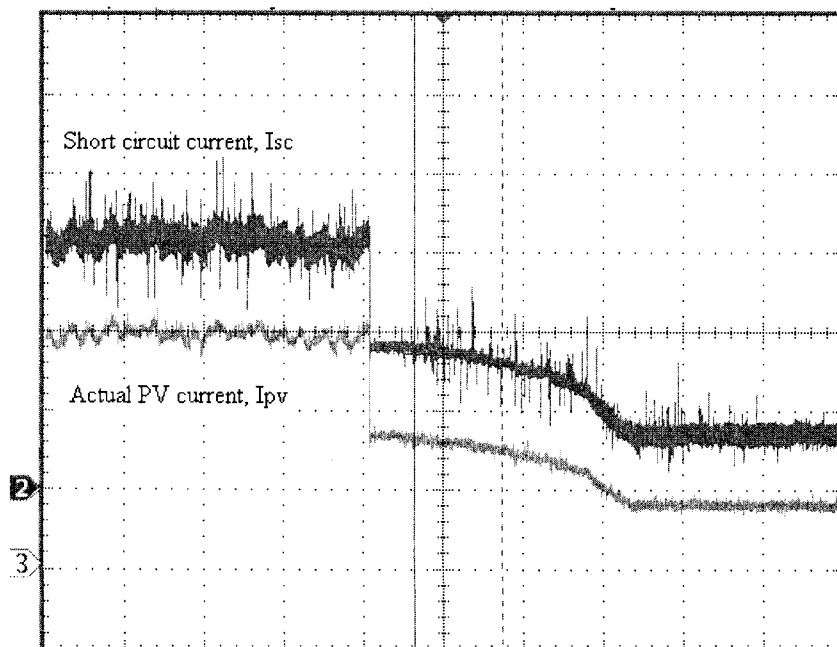
Time Scale: 1s/Div; Vertical Scale: 1V/Div

Figure 4-14: Waveform of I_{PV} Tracking I_{SC}

53
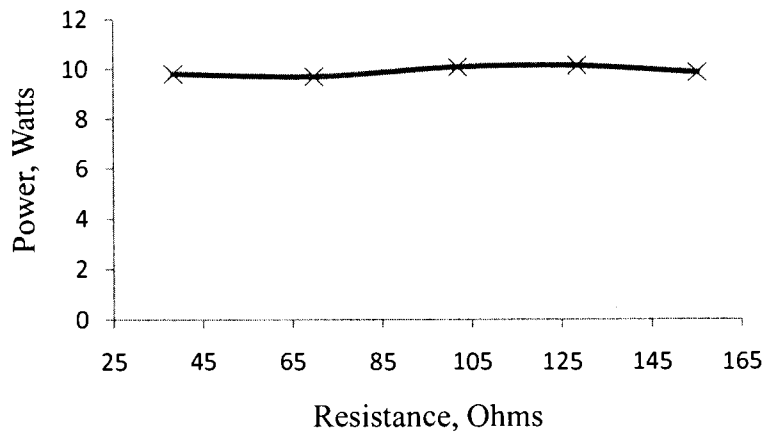
Figure 4-15: PV Power Versus Load

4.4. Inverter and Slip Control of DFIG

4.4.1. DFIG Characteristics

The rotor terminals of a DFIG are accessible so it is possible to apply a three-phase voltage with varying magnitude and frequency (f_r) into the rotor circuit. An AC voltage of frequency f_r applied to a standstill rotor will generate a flux with frequency f_r. However, if the rotor is rotated with a mechanical frequency of f_m, then the net flux linkage of the rotor will have a frequency be equal to $f_r + f_m$. In order to maintain the frequency of the induced stator voltage at 60 Hz, the net flux linkage of the rotor must be maintained at 60 Hz, i.e., $f_r + f_m = f_s$, where f_s is the stator frequency (60Hz). The rotor mechanical frequency, f_m, will change with changing wind speeds which means that in order to keep $f_r + f_m$ constant, f_r of the injected voltage should be changed.

The induced stator voltage is related to the rotor voltage by [31]:

$$V_s = \frac{V_r}{s} * a \qquad (4.8)$$

54

$$s = \frac{f_r}{f_s}$$ (4.9)

where V_s is the stator voltage, V_r is the rotor voltage, a is the ratio of the number of turns in the stator windings to the number of turns in the rotor windings and s is the slip. According to (4.8), an increase in the mechanical speed of the rotor will result in an increase in the magnitude of the stator voltage.

The stator power, P_s, and the injected rotor power, P_r, are related by the following expression:

$$P_r = s * P_s.$$ (4.10)

In an induction motor, the synchronous speed $N_s = 120f_s/P$ where f_s is the rated frequency (60 Hz) and P is the number of poles. At sub-synchronous speeds ($N_m \leq N_s$), the slip is positive and P_r, also called the slip power, is positive. This means that the inverter will inject power into the rotor. At speeds above the synchronous speed ($N_m \geq N_s$), P_r will be negative which means that the rotor-side power converter operates in the rectifier mode and absorbs slip power from the rotor.

In this work, a three-phase Sine PWM inverter is used to convert the DC voltage from the three-phase PFC/ PV boost converter to a three-phase AC voltage for rotor injection. A slip and constant volts/Hz control scheme [31] is used to control the rotor injection so as to maintain the DFIG stator voltage at a constant magnitude and frequency. The rotor speed data of the DFIG is provided using a digital speed transducer and is used by the PWM controller to calculate the slip.

4.4.2. PSIM Simulation

The system is simulated using PSIM as shown in Figure 4-16. The three-phase PFC provides a fixed DC link voltage for the inverter. The four pole wound rotor induction

55

machine (IM) has a synchronous speed of 1800 rpm and the IM stator feeds an isolated three-phase wye-connected 21-ohm resistive load. The simulation parameters for the induction machine are shown in Table 4-4. A DC motor is coupled to the shaft of the IM and is used to emulate the wind turbine. The shaft speed is adjusted by changing the DC motor armature voltage and this is done to represent changes in wind speed.

The Sine PWM control scheme is shown in the lower part of Figure 4-16. The shaft speed information is fed into the controller which than uses the information to calculate the slip. The sinusoidal control signals ($\hat{V}_{control}$) are generated from a DQ0-ABC block and will have the same frequency as the rotor injection voltage. The inputs to the DQ0-ABC block are the phase angle and the DC voltage magnitude. The DC voltage magnitude is controlled by the slip. The rotation angle θ is obtained by integrating the slip frequency. The Q0 inputs to the block are tied to ground and so the transformation from a DC voltage is given by:

$$V_{abc} = \begin{bmatrix} cos\theta & sin\theta & 1 \\ cos\left(\theta - \frac{2\pi}{3}\right) & sin\left(\theta - \frac{2\pi}{3}\right) & 1 \\ cos\left(\theta + \frac{2\pi}{3}\right) & sin\left(\theta + \frac{2\pi}{3}\right) & 1 \end{bmatrix} \begin{bmatrix} V_{dc} \\ 0 \\ 0 \end{bmatrix}. \tag{4.11}$$

The frequency of the triangular wave carrier signal is set at 20 kHz and the amplitude ($\hat{V}_{tri}$) is set at 100 V. The amplitude modulation ratio m_a is defined as:

$$m_a = \frac{\hat{V}_{control}}{\hat{V}_{tri}}. \tag{4.12}$$

The injected rotor per phase voltage is given by [30]:

$$\hat{V}_{r\_an} = m_a * \frac{V_{DC-link}}{2}. \tag{4.13}$$

The stator voltage and rotor voltage are related by:

$$|V_s| \approx \frac{|Vr|}{s}. \tag{4.14}$$

Note that $\hat{V}_{control}$ is a function of slip so if the speed of the shaft changes, m_a will be automatically adjusted to change the injected rotor voltage magnitude and maintain a constant stator voltage.

The system is tested for sub-synchronous operation at two different "wind speeds" to verify if the control algorithm is able to maintain constant frequency and magnitude for the stator voltage. The DC motor armature voltage is adjusted to 1012 RPM and then to 750 RPM. The results are summarized in Table 4-5. The waveforms of stator voltage, rotor injection current, DC link voltage, stator output power and rotor injection power are shown for both cases in Figure 4-17 to Figure 4-20.

Table 4-4: Induction Machine Simulation Parameters

Stator resistance, R_s	0.294 Ω
Stator leakage inductance, L_s	1.39 mH
Rotor resistance, R_r	0.156 Ω
Rotor leakage inductance, L_r	0.74 mH
Magnetizing inductance, L_m	41 mH
Turns Ratio, N_s/N_r	1
Number of Poles, P	4
Moment of Inertia, J	0.4 Kg.m^2

Table: 4-5: Simulation Results

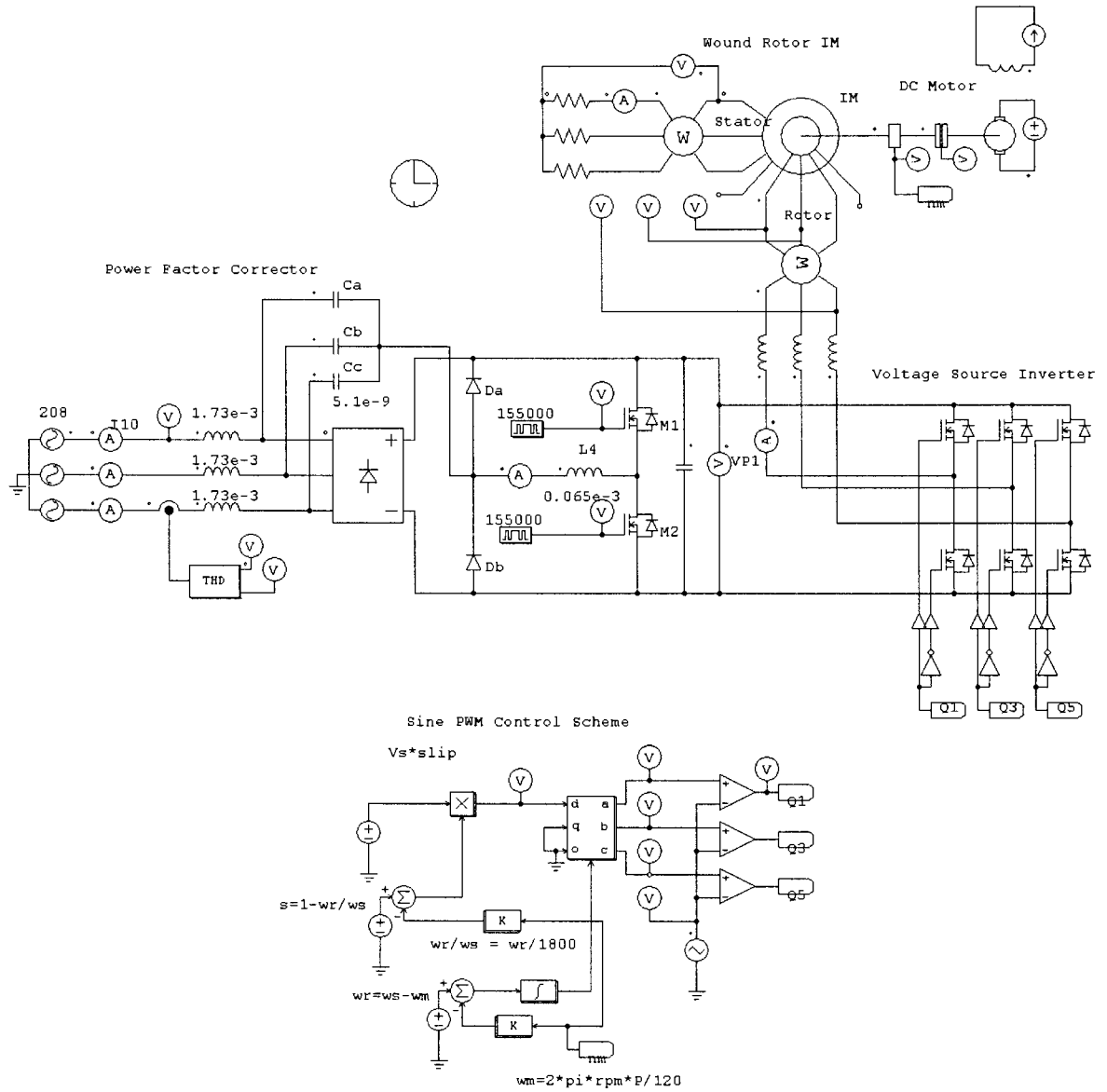| Shaft Speed (RPM)	1012	750
Slip, s	0.44	0.58
Mechanical frequency, f_m (Hz)	33.67	25.00
Rotor Frequency, f_r (Hz)	26.30	35.00
Stator Frequency, f_s (Hz)	60	60
Stator phase-to-neutral voltage, V_{s-an}	119	118
$V_{DC-link}$	282	282
Stator output power (Watts)	1979	1953
Rotor Injection Power (Watts)	877	1129

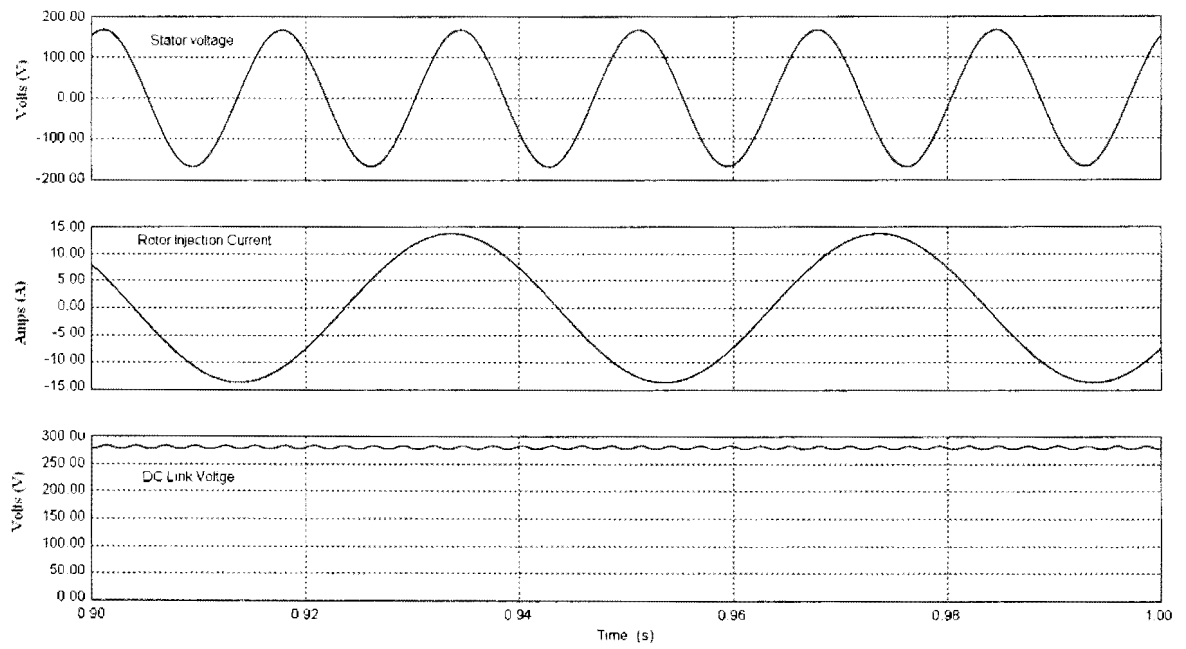*Figure 4-16: Simulation Diagram of DFIG System*

Figure 4-17: Waveforms of Stator Voltage, Rotor Injection Current and DC Link Voltage at 1012 RPM
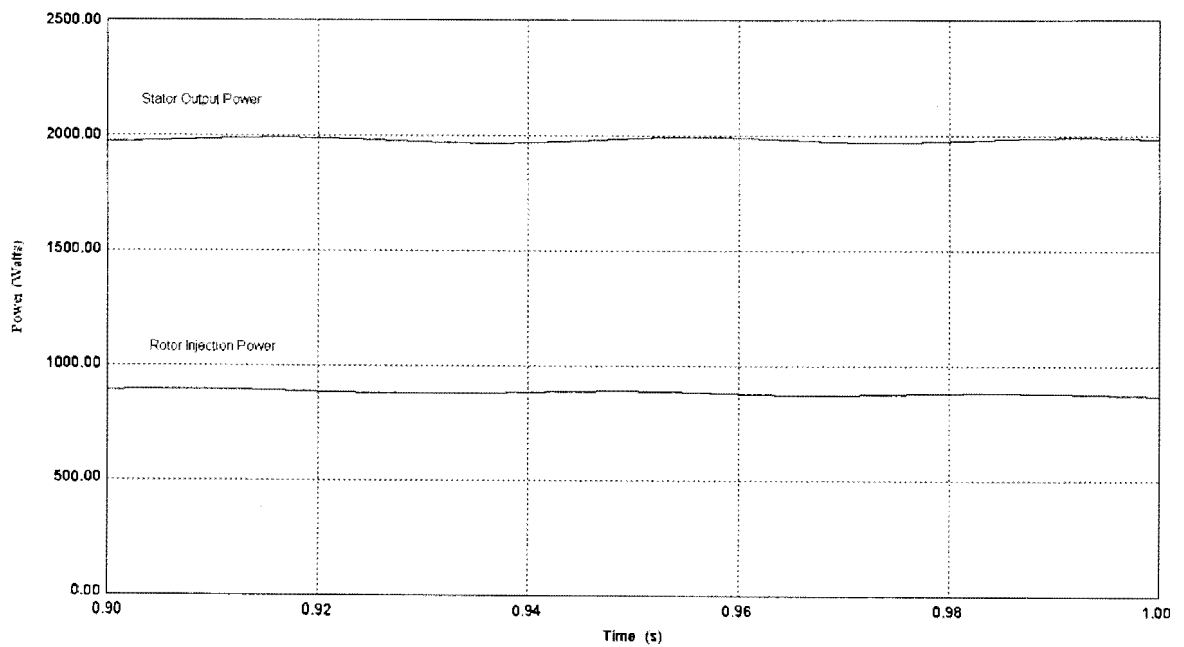

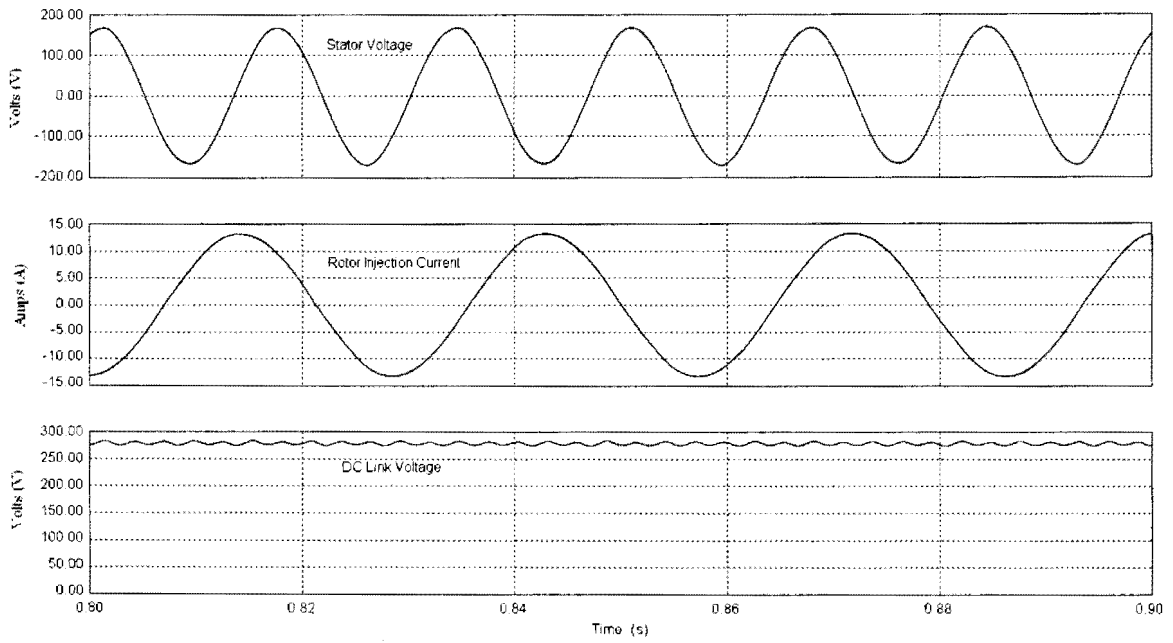*Figure 4-18: Stator Power and Rotor Injection Power at 1012 RPM*

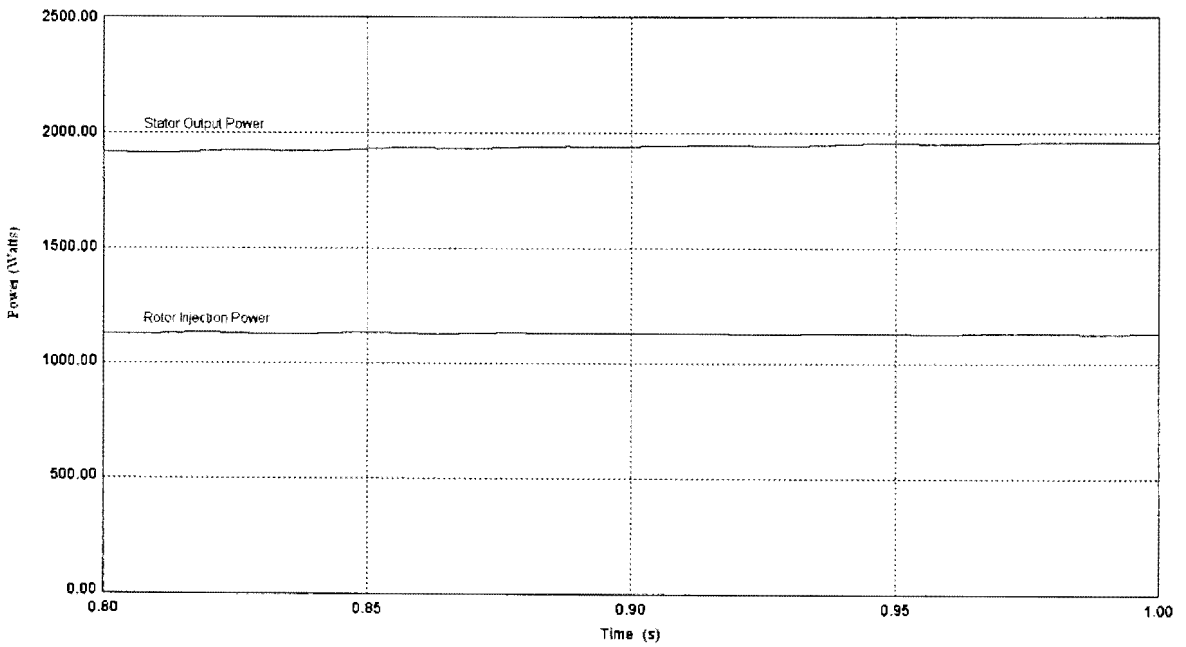*Figure 4-19: Waveforms of Stator Voltage, Rotor Injection Current and DC Link Voltage at 750 RPM*

Figure 4-20: Stator Power and Rotor Injection Power at 750 RPM

60

The simulation results verify the effectiveness of the control system. The PFC provides a constant DC link voltage for the inverter. It is shown that the rotor injection is effectively controlled to maintain a stator voltage with constant frequency and magnitude for both shaft speeds. A stator output power of roughly 2 kW is obtained for both cases and the rotor injection power is equal to slip times stator power (4.10).

4.4.3. Experimental Setup

This section presents a dsPIC-controlled three-phase wound-rotor induction motor (DFIG) operating under sub-synchronous conditions with an isolated resistive load. In the experimental setup, a 5HP 4-pole wound rotor induction motor is used as the DFIG. A separately excited DC motor is used as the prime mover substituting the wind turbine. An isolated wye-connected 21 ohm three- phase load is connected to the stator of the induction machine. An IGBT Power Electronics system module from Semikron is used to build the power circuit of the PWM inverter [32]. This module integrates all the driver circuits, six IGBTs for the three phase inverter, protection circuitry and power filtering into a single module. The gate pulses for the IGBT module are supplied by the dsPIC after being stepped up to the voltage level of 15V. The rotor shaft speed is supplied to the dsPIC using a non-contact optical tachometer which is capable of detecting a reflected pulse from a rotating shaft pasted with a reflective tape. The DC voltage supplied is converted into an AC voltage with a variable frequency and magnitude which is fed to the rotor of the induction machine. The frequency and magnitude of the rotor injection voltage is controlled by the dsPIC in order to maintain the magnitude and frequency of the stator voltage constant. Figure 4-21 shows the block diagram of the experimental setup.
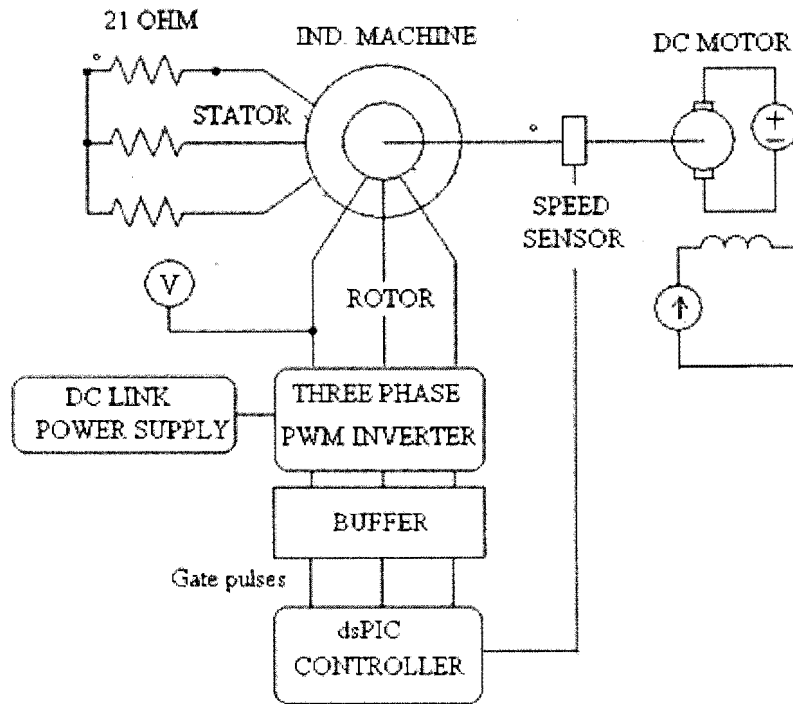
Figure 4-21: Block Diagram of the dsPIC Controlled DFIG

4.4.4. dsPIC Implementation

DSC Source Code

All the programming for the DSC was done in C language in the MPLAB IDE. The code files used and a brief description of each are provided in Table 4-6.

Table 4-6: Description of DSC Code Files

File name	Type	Description
dfig_final.c	Source File	Main software routine
function.c	Source File	Source code for routinely used operations
cosine.h	Header File	Sine wave lookup table
amp_mode.h	Header File	Scaling table for amplitude Modulation
math.h	Header File	Header file for basic mathematical operations
p30F2020.h	Header file	DSPIC header file
p30f2020.gld	linker script	DSPIC linker script

The main function for the dsPIC controller is to adjust the rotor injection such that the stator voltage (both frequency and magnitude) is maintained constant for different wind turbine speeds. In conventional three-phase Sine PWM implementation, three sinusoidal phase voltages (control signals) are compared to a triangle wave carrier signal in order to generate the PWM signals. The PWM signals are pulse trains with fixed frequency, fixed magnitude but with varying pulse width. In order to implement this scheme, hardware circuits are required to generate the control and carrier signals. In this project, the dsPIC MCPWM module is used to generate the gate signals and Sine PWM is implemented entirely using software. This section briefly describes how a three-phase sine wave of varying frequency and magnitude for rotor injection can be generated with the dsPIC.

Three of the four available PWM generators from the dsPIC MCPWM module are used (Figure 4.22). The fourth generator is reserved for providing gate pulses to the PFC circuit. The MCPWM module is configured so that each generator outputs a pair of signals which are complimentary to each other. A small dead time is inserted between the complementary pulses during which both switches PWMxH and PWMxL are off thereby preventing shoot through. The PWM frequency is chosen to be 20 kHz which is outside the audible noise range.

Three-Phase Sine Wave Generation with Lookup Table

In the dsPIC MCPWM module, the PDC register holds the duty cycle information for the PWM Generator. For this project, a PDC value of 0 corresponds to 0% duty cycle and 32,000 corresponds to 100%. Once the PDC register is written with a value within the specified range, the module will automatically adjust the duty cycle of the PWM pulse to
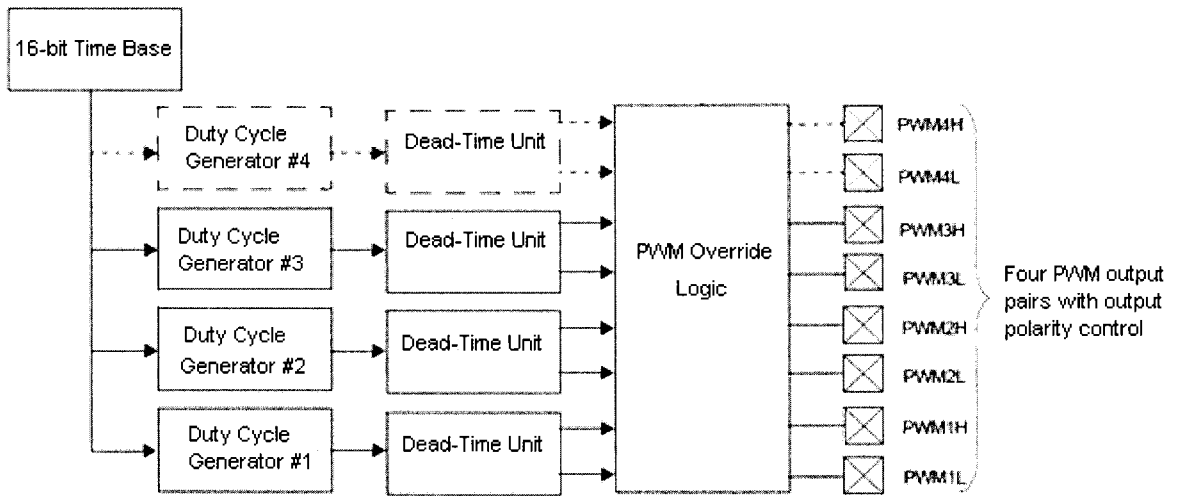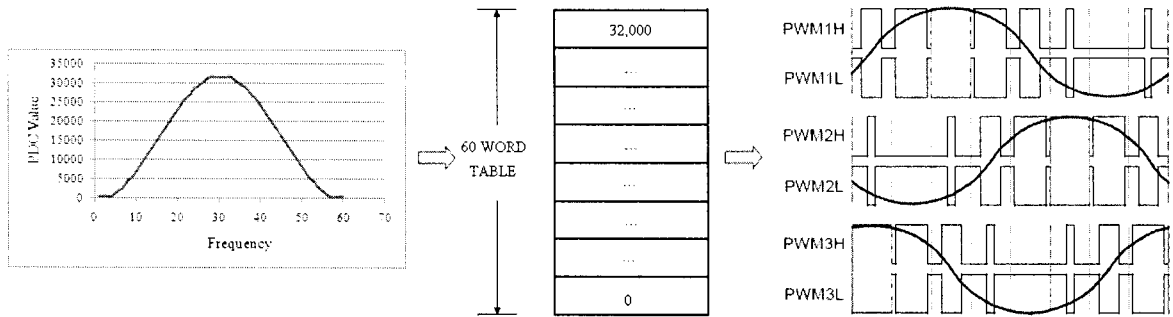
Figure 4-22: Block Diagram of MCPWM

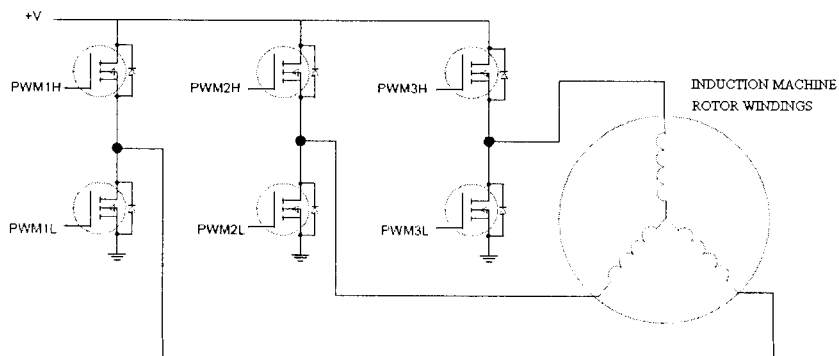*Figure 4-23: Three-Phase Sine Wave Generation with Lookup Table*

Figure 4-24: Three-Phase Inverter

64

match that value. To generate a single-phase sine wave for phase '*a*', sinusoidal data for a complete electrical cycle is provided by a 60 word table. A pointer (called PDCa) in the software is then used to step through the table at a certain rate. Sine wave outputs for phase '*b*' and '*c*' are then obtained by simply offsetting the starting position of the respective pointers (PDCb and PDCc) by 120° and 240°. Figure 4-23 shows the lookup table and the three sine waves obtained with the PWM module. Here, PWM1H represents the gate signal to the high-side switch for phase '*a*' of the three-phase inverter (Figure 4.24) and PWM1L represents the gate signal to the low side. Similarly, PWM2X represents phase '*b*' and PWM3X represents phase '*c*'.

The frequency of the sine wave is then easily controlled by changing the rate at which the pointer steps through the table. Adjusting this step-through rate is thus equivalent to frequency modulation. Similarly, the amplitude of the sine wave is adjusted by scaling the values in the PDC duty cycle lookup table. This is equivalent to amplitude modulation.

Figure 4-25 shows the flow chart of the source code. The dsPIC first calculates the rotor shaft speed. The INT1 interrupt works in conjunction with the Timer2 interrupt to determine the shaft speed. Timer2 is set to trigger once every 10 μs and increments period counter variable, *k*, of the speed sensor. The speed sensor sends a 5 V pulse to the dsPIC each time the shaft makes a complete revolution and the INT1 interrupt is triggered on the rising edge of these pulses. Each time the INT1 interrupt is triggered, it records the number of 10 μs counts for each complete revolution of the shaft and sends this information to the main routine. The main routine then uses this information to determine the required rotor injection frequency using the following equations:

$$Nm = \left(\frac{100,000}{k}\right) * 60 \tag{4.15}$$

$$fm(Hz) = Nm * \frac{P}{120} = 2 * Nm \qquad (4.16)$$

$$fr(Hz) = 60 - fm = 60 - 2 * Nm(RPM) \qquad (4.17)$$

where *Nm* is the shaft speed in RPM, *k* is the speed sensor period count, *fm(Hz)* is the electrical shaft frequency, *P* is the number of poles of the machine (4), and *fr(Hz)* is the required rotor injection frequency.

Frequency Control

As mentioned previously, the sinusoidal frequency is controlled by varying the rate at which the pointer steps through the sine lookup table. The pointer steps to the next value in the lookup table each time the Timer1 interrupt service routine is implemented. Therefore, in order to change the step-through rate, the Timer1 interrupt period needs to be changed. For example, in order to increase the sine wave frequency, the Timer1 interrupt period is decreased and vice versa. Adjustments to the Timer1 interrupt period are made by writing to its period register PR1. PR1 is related to *fr* by the following equation:

$$PR1 = \frac{41666.67}{fr(Hz)} + \frac{1}{2}. \qquad (4.18)$$

For example, for a desired rotor injection frequency of 30 Hz, PR1 must be set to 1388.

Amplitude Control

The amplitude modulation is slip based in that, for a given rotor shaft speed, the amplitude of the rotor injection voltage is adjusted to keep the stator voltage constant. It is seen from equation (5), that an increase in the mechanical speed of the rotor will increase the magnitude of the stator voltage. Therefore, for higher speeds, the rotor voltage must be decreased and vice versa. The average output voltage from the inverter is changed by scaling all the values in the lookup table. The scaling factor will be referred to as

amp_scale. A second lookup table is created to store *amp_scale* values for different slips. For example, if the rotor shaft speed increases, then the rotor injection voltage must be reduced which means that all the values in the lookup table have to be scaled down by a certain *amp_scale* factor.

A calibration experiment was carried out to determine the *amp_scale* scaling factors for different values of slip for the induction machine. This calibration was done under the following conditions:

1) The DC link voltage was maintained at 40 VDC.

2) The wind turbine speed was adjusted from 200 RPM to 1500 RPM.

3) The stator voltage was maintained at $30V_{L-L}$ (note: a small value was chosen for safety reasons but stator voltage can easily be scaled up).

Figure 4-25 shows the calibration curve. The linear equation obtained from the curve fitting was used to generate the *amp_scale* lookup table. In the software, the main routine computes the slip and Timer3 interrupt uses this slip value to pick the correct amplitude scaling factor from the *amp_scale* table. The Timer3 interrupt is set to trigger once every 250 μs. The flowchart for DFIG control using the dsPIC is shown in Figure 4-26.

4.4.5. Experimental Waveforms

Figure 4-27 shows waveforms of the rotor current and stator voltage (line-to-line) with the shaft rotating at 1230 RPM, the DC link voltage set at 44V and a three-phase wye-connected resistive load. An RMS voltage of approximately 120V at 60 Hz is obtained. It should be noted that the amplitude scaling in the controller was calibrated to maintain a constant stator voltage of 30V with a 60 Hz frequency. It is seen that the rotor injection is automatically adjusted for different shaft speeds to maintain V_s constant. Figure 4-28

67

shows the variation of V_s with shaft speed and it is seen that V_s remain fairly constant at an average value of 29.6V. Figure 4-29 shows the waveforms of the rotor current (I_r) and stator voltage (V_s) for different shafts speeds.
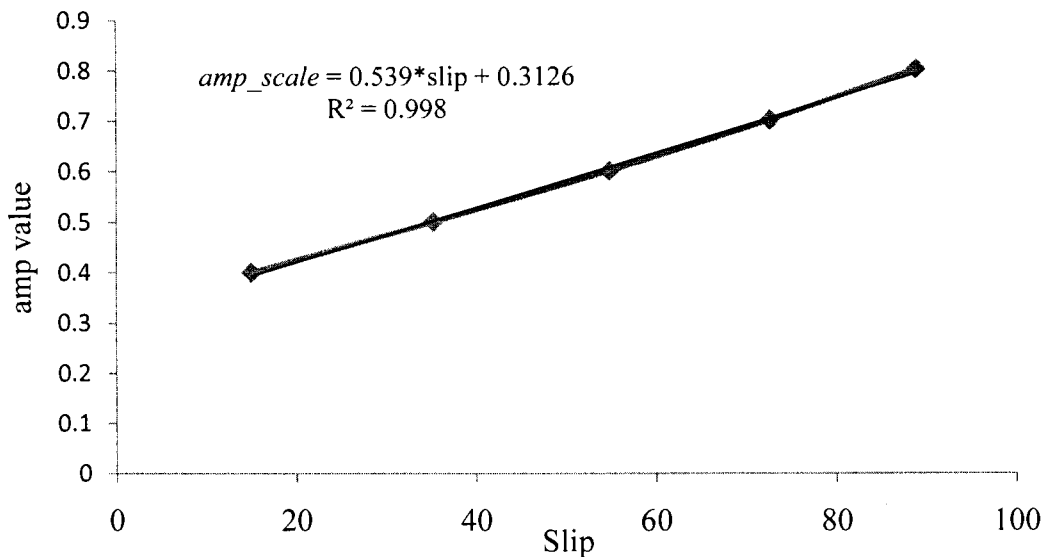
Figure 4-25: Calibration Curve Relating Amp_scale and Slip

4.5. Conclusions

This chapter presents a hybrid DFIG-based wind energy system with an efficient rotor injection scheme with the possibility of providing the injection power from either three-phase AC mains or PV panel-battery combination. A PFC circuit is used as the grid-side AC-DC converter and has features like unity power factor, zero voltage switching (ZVS) and high efficiency. The boost converter used to feed PV power to the rotor does not use any additional switches thereby resulting in a simpler power circuit. A current based MPP tracking system is implemented using a DSC to ensure that maximum available power is extracted from the PV panels. A three-phase Sine PWM inverter is used to convert
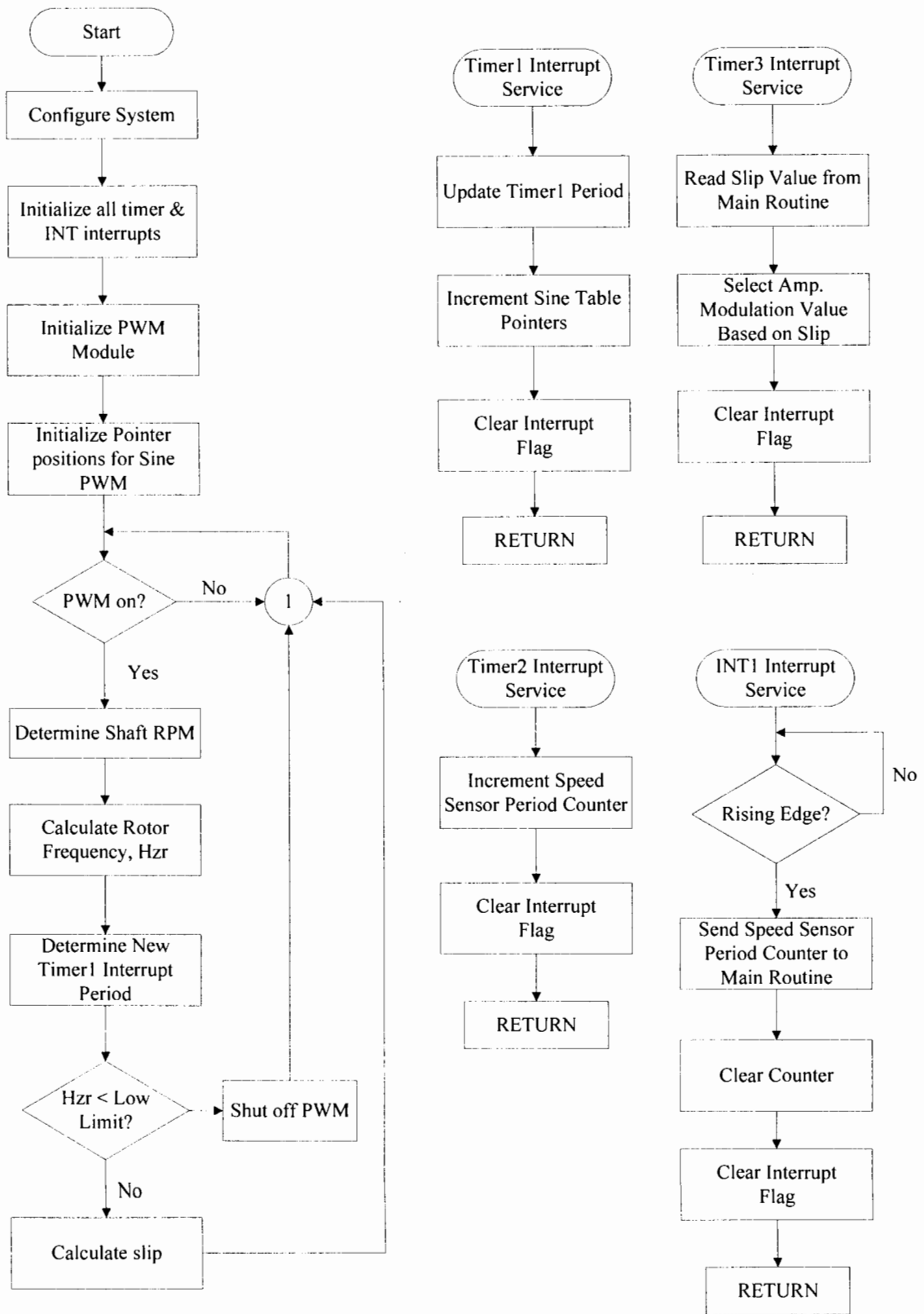
Figure 4-26: Flowchart for DFIG Control dsPIC Coding
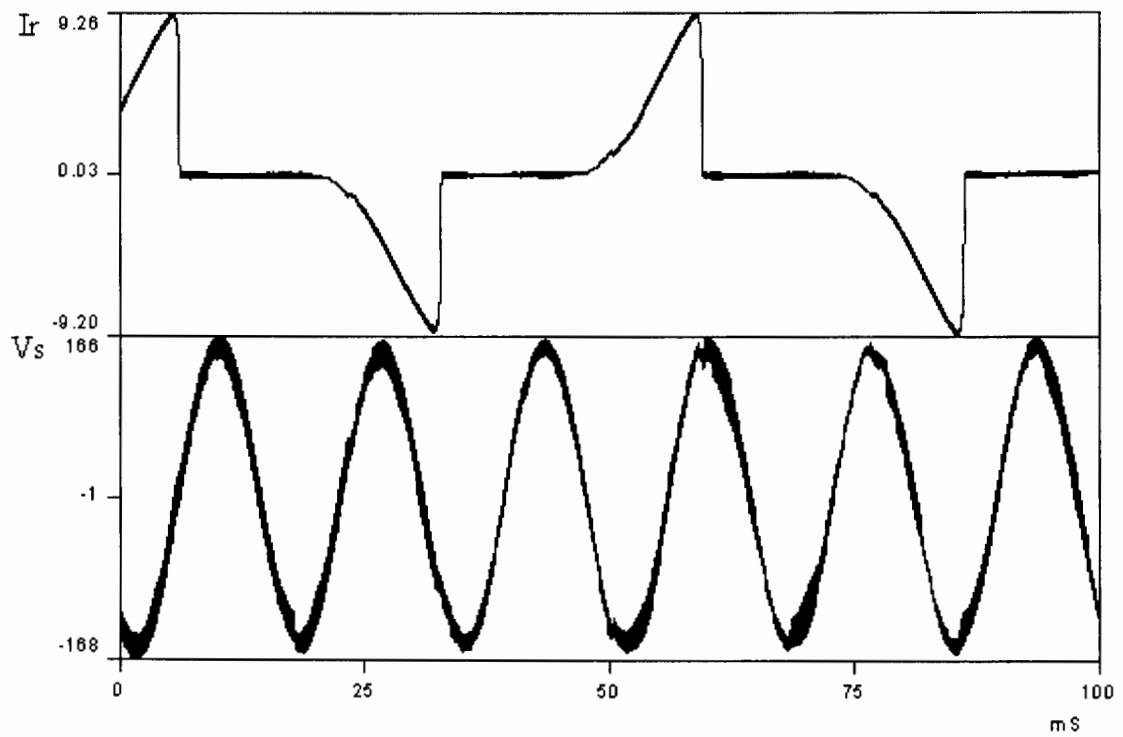
Figure 4-27: Waveforms of Rotor Current and Stator Voltage
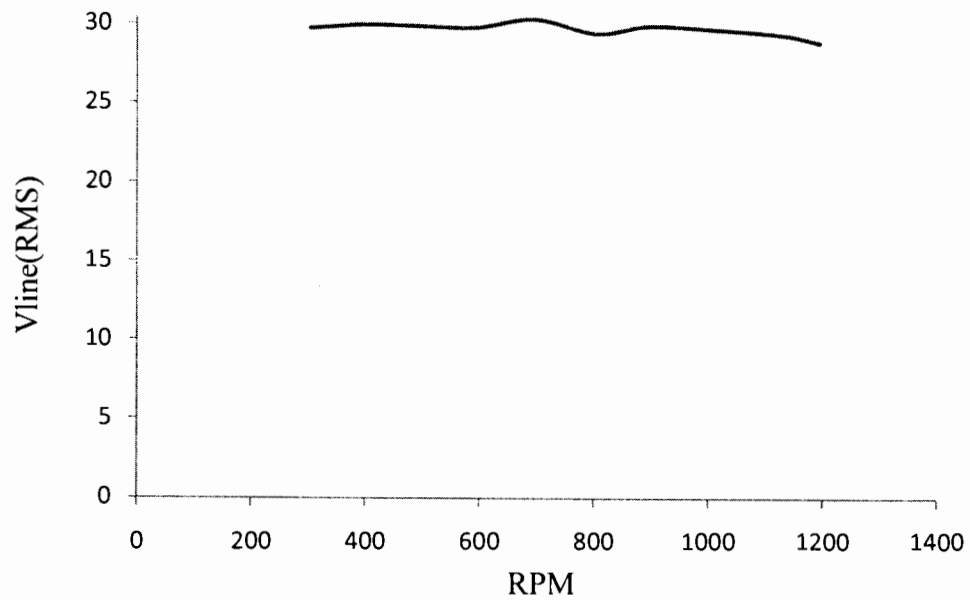
Figure 4-28: Variation of Stator Voltage with Shaft Speed

70
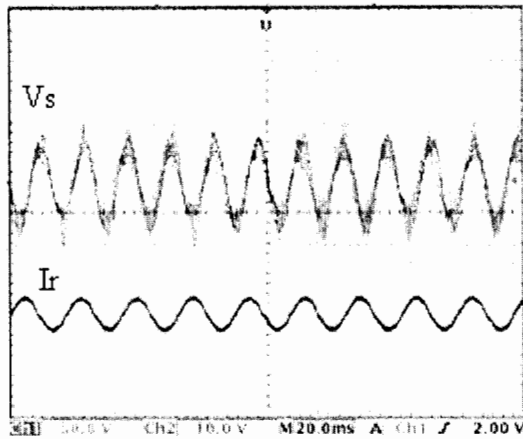
(a)

Nm = 400 RPM, fm = 13.33 Hz,
fr = 46.67 Hz, fs = 60Hs, Vs = 30V
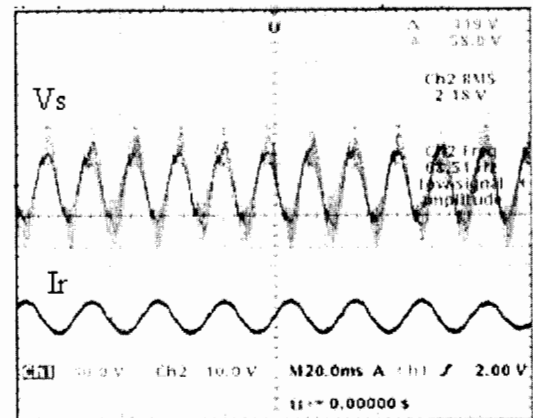
(b)

Nm = 600 RPM, fm = 20 Hz, fr = 40 Hz,
fs = 60Hz, Vs = 30V
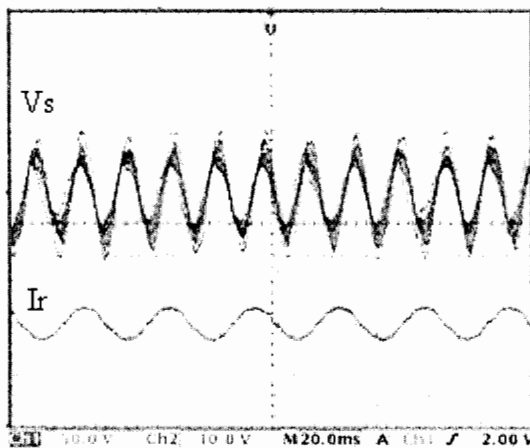
(c)

Nm = 800 RPM, fm = 26.67 Hz,
fr = 33.33 Hz, fs = 60 Hz, Vs = 30V
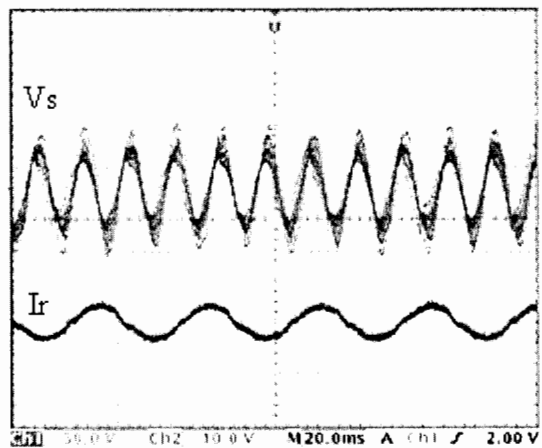
(d)

Nm = 1000 RPM, fm = 33.33 Hz,
fr = 26.67 Hz, fs = 60 Hz, Vs = 30V

Figure 4-29: Waveforms of Rotor Current and Stator Voltage for Different Rotor Shaft Speeds

71

the DC voltage from the three-phase PFC/ PV converter into a variable-frequency AC voltage that is injected into the rotor of the DFIG. A digital speed transducer provides pulses with frequency proportional to the rotor speed. The DSC processes the data and provides gate pulses to the PFC and the inverter.

The hybrid power converter system proposed in the thesis is useful in combining wind energy and solar energy such that the wind energy constitutes the bulk of the power produced while the solar (PV) panels provide a fraction of the power through rotor excitation. However, when there is no sunlight, the system in the present form can supply power only for a limited amount of time because of the battery. This can be overcome by adding an auxiliary circuit for charging the battery from the three-phase AC mains. The proposed system will operate only at sub-synchronous speeds where the inverter injects power into the rotor. However, at super-synchronous speeds, the rotor power flow is reversed. In this case the rotor-side converter can be used as a rectifier and the excess power from the DFIG rotor could be used to charge the battery.

CHAPTER 5. MULTILEVEL CASCADE INVERTER FOR HYBRID RENEWEWABLE ENERGY SYSTEMS

5.1. Introduction

The basic function of multilevel inverters is to use a series of power semiconductor switches to synthesize an AC voltage waveform from several lower level DC voltages. Multilevel inverters are gaining increasing attention for use in renewable energy systems because sources such as photovoltaics, wind, and fuel cells can easily be interfaced to multilevel converter systems [33]. Multilevel inverters are modular and scalable and therefore well suited for systems where there is potential for future growth. For example, in multilevel inverters, additional PV panels can easily be added into an existing PV system. Furthermore, they can achieve high power ratings and reach high voltage with low harmonics without using any transformers.

Advantages of Multilevel Inverters

Multilevel inverters offer many advantages over the conventional 3-level PWM inverters:

- Generate staircase waveforms with very low distortion.

- Draw input current with low distortion.

- Can operate at fundamental switching frequencies. Lower switching frequency usually means lower switching loss and higher efficiency.

- Operating at lower switching frequency can reduce the dv/dt stresses; therefore electromagnetic compatibility (EMC) problems can be reduced.

- Common-mode (CM) voltage: Wind energy applications typically use PWM power inverters with high frequency switching. Common mode voltage generated by

power inverters in high frequency applications can cause unwanted problems such as shaft voltage and bearing currents which cause premature bearing failures in electric machines [34]. Multilevel converters produce smaller CM voltage so the stress on the bearings of a motor connected to a multilevel motor drive will be reduced.

- Banks consisting of batteries or large capacitors which are connected as DC sources can provide static var compensation and also provide ride through capability for voltage sags or load swings experienced at the utility interface connection [35].

Disadvantages of Multilevel converters

- Typically require a large number of switches.

- Require complex gate drive circuits.

There are various kinds of multilevel converters. The most commonly discussed in literature are:

- Multilevel Cascaded H-bridges Inverter (MCHBI).

- Diode-Clamped Multilevel Inverter.

- Flying Capacitor Multilevel Inverter.

The MCHBI is considered for this project because it is modular and scalable and well suited for renewable energy applications. Furthermore a simple fundamental switching scheme can be utilized to generate AC voltages.

5.2. The Multilevel Cascaded H-Bridge Inverter (MCHBI)

The configuration of a single phase full-bridge inverter unit, or H-bridge, is shown in Figure 5-1(a). The H-bridge connected to the DC source of voltage V_{DC} consists of four switches S_1, S_2, S_3 and S_4, which are controlled such that the output voltage, V_{ab}, of the inverter has three levels: $+V_{DC}$, 0, or $-V_{DC}$. The switching states and output voltage for each state is summarized in Table 5-1.

Table 5-1: Switching States for H-Bridge

S_1	ON	ON	OFF	OFF
S_2	OFF	ON	OFF	ON
S_3	OFF	OFF	ON	ON
S_4	ON	OFF	ON	OFF
V_{ab}	$+V_{DC}$	0	0	$-V_{DC}$

The MCHBI is shown in Figure 5-1(b) where a total of s H-bridge inverters are tied in series with each H-bridge using a separate DC source. The output of the MCHBI is the sum of the outputs all the individual inverter and, therefore, a staircase waveform can be synthesized by controlling the output of each H-Bridge. This is illustrated in Figure 5-2 which shows the output waveform of an MCHBI consisting of three H-bridges, each with its own DC source. For this example, each DC source is assumed to have a constant voltage equal to V_{DC} which means that each inverter has three discrete output levels: $+V_{DC}$, 0, or $-V_{DC}$. When S_1, S_2, S_3 and S_4 for each H-bridge are turned on and off, the waveforms for each H-bridge can be shaped as in Figure 5-2 and when added in series, an output staircase waveform is produced. The number of voltage levels m in an MCHBI with s DC sources is $m = 2s+1$. Figure 5-2 shows a seven level staircase waveform. As the number of voltage levels increases, the staircase waveform will better resemble a true sinusoidal output.

75
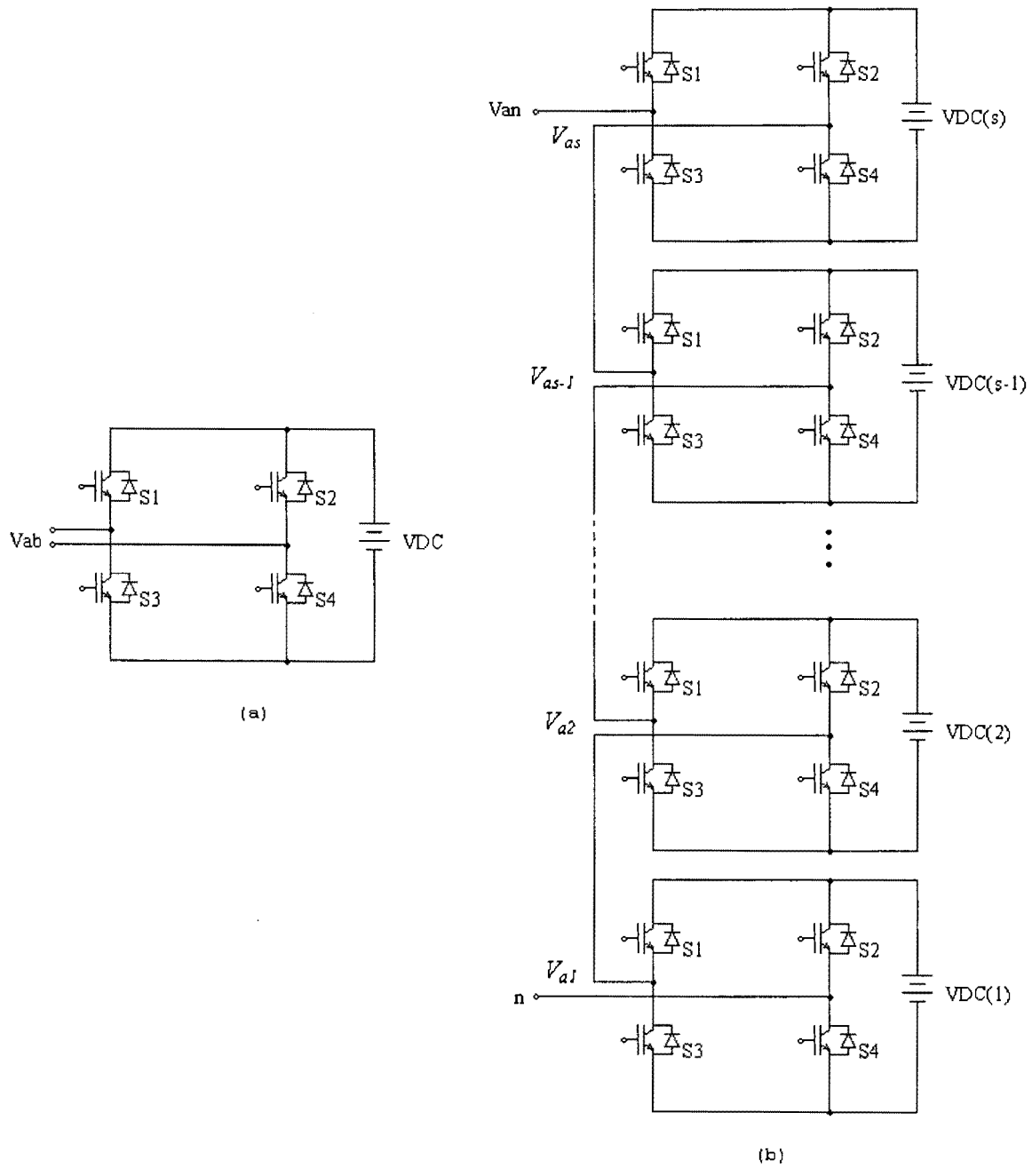
Figure 5-1: (a) Single H-Bridge Configuration, (b) Single Phase of a MCHBI

76
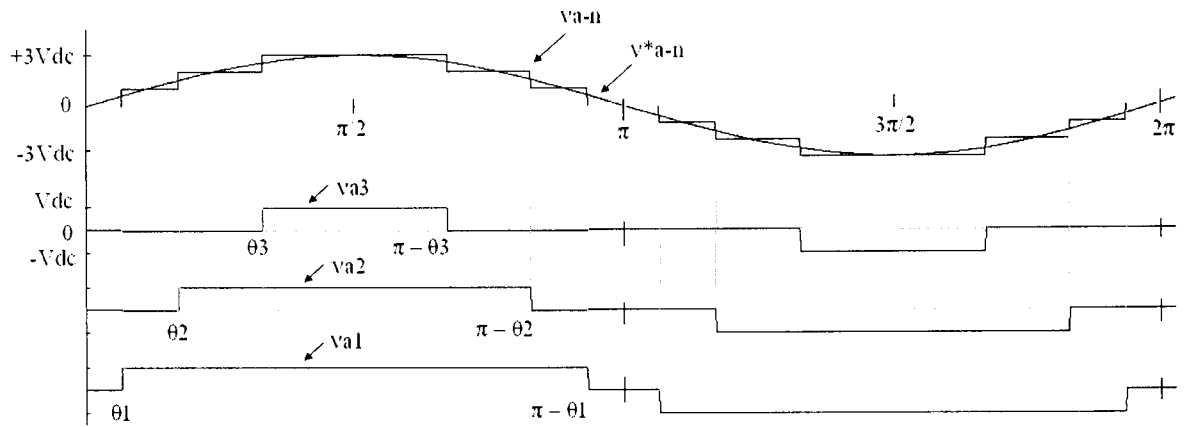
Figure 5-2: Output Waveform for a 3-step, 7-Level MCHBI

5.2.1. Fourier Analysis

The staircase output waveform of the MCHBI can be analyzed using Fourier analysis. The Fourier series of the waveform with separate unequal DC sources can be written in general form as [36]:

$$V(\omega t) = \sum_{h=1,3,5,\ldots}^{\infty} \frac{4}{\pi}[V_1\cos(h\theta_1) + V_2\cos(h\theta_2) + \ldots + V_s\cos(h\theta_s)]\frac{\sin(h\omega t)}{h} \qquad (5.1)$$

where h is the odd harmonic number, s is the number of DC sources, V_1, V_2, ...V_s are the magnitudes of the dc voltage sources and θ_1, θ_2, ...θ_s are the switching angles (Figure 5-2).

5.2.2. Switching Algorithm and Selective Harmonic Elimination

Various pulse width modulation (PWM) strategies are used in multilevel converters [33]. In this work, a fundamental switching scheme is used where the switching frequency of each of the IGBTs matches the frequency of the fundamental component of the AC waveform. The main challenge with using the fundamental switching scheme is the selection of the correct switching angles (times) for each switch such that (a) only the fundamental voltage is produced and (b) certain specifically chosen lower order harmonics are eliminated. Once the lower order harmonics have been eliminated, higher order

77

harmonics can easily be filtered out using filters with smaller component values. In the following sections, a method of selecting the switching angles for an MCHBI with s = 3 is described for two different cases. The analysis is first done for an MCHBI with three DC sources ($s = 3$).

In the first case, the DC sources are assumed to have equal magnitudes and the switching angles are selected to eliminate the 5th and 7th harmonics. It is to be noted that the triplen harmonics do not have to be eliminated since they cancel each other out in the line-to-line voltage in three phase applications. One phase of the three-phase MCHBI is simulated with the calculated switching angles and the waveforms are analyzed. In the second case, DC sources assumed to have different magnitudes. This condition is more representative of a realistic case where, for example, batteries are connected as the DC sources. However, to simplify the analysis, the DC sources take on only certain discrete values. The rationale for choosing these values will be explained later.

Case 1: Analysis with Equal DC Sources

The DC sources (total number = 3) are assumed to be equal and are normalized to unity. Then, from (5.1), a system of non-linear transcendental equations is obtained:

$$\cos(\theta_1) + \cos(\theta_2) + \cos(\theta_3) = K$$
$$\cos(5\theta_1) + \cos(5\theta_2) + \cos(5\theta_3) = 0 \tag{5.2}$$
$$\cos(7\theta_1) + \cos(7\theta_2) + \cos(7\theta_3) = 0$$

$$K = \frac{\pi V_p}{4}$$

where V_p is the desired peak value of the fundamental component (normalized to V_{DC}). The system of non-linear transcendental equations is solved using an iterative method. The

Newton-Raphson algorithm shown in Figure 5-3 was used in MATLAB and the switching

angles obtained for $V_p = 3V$ are shown in Table 5-2.

Table 5-2: Switching Angles for MCHBI (s = 3)

```
%---------------------------------------------------------------------------
%Newton_Raphson Algorithm for solving for the switching angles to
eliminate the 5th and 7th %harmonics for a 3 step, 7 level Multi-level
inverter.
%Munir Kaderbhai 09/10/09
%---------------------------------------------------------------------------

Dx = [10;10;10];                                  %Change in variable is
                                                  %set to a high value.
x = [0.192011; 0.541122; 1.012422];               %Initial Estimate.
C = [2.35;0;0];                                   %C is desired Vp value.
iter = 0;                                         %Iteration counter.
while max(abs(Dx))>=0.0001 & iter <10000;         %Test for convergence.
    iter = iter+1;                                %No. of iterations.

F = [cos(x(1)) + cos(x(2)) + cos(x(3));
     cos(5*x(1)) + cos(5*x(2)) + cos(5*x(3));
     cos(7*x(1)) + cos(7*x(2)) + cos(7*x(3))];

DC = C-F;
J = [-sin(x(1)), -sin(x(2)), -sin(x(3));           %Jacobian matrix.
     -5*sin(5*x(1)), -5*sin(5*x(2)), -5*sin(5*x(3));
     -7*sin(7*x(1)), -7*sin(7*x(2)), -7*sin(7*x(3))];

Dx = J\DC;
x = x+Dx;
end

y = x*((360)/(2*pi))
%---------------------------------------------------------------------------
```

Figure 5-3: Newton-Raphson Algorithm for Switching Angles

Table 5-2: Switching Angles for MCHBI (s = 3)

θ3	58.58°
θ2	31.18°
θ1	11.68°

The MCHBI is simulated in PSIM with the switching angles given in Table 5-2 and

the staircase waveform obtained is shown in Figure 5-4 along with the fundamental

79

component of the waveform. Figure 5-5 shows the frequency spectrum of the waveform in which the 5th and 7th harmonics have been successfully eliminated and the fundamental voltage has the desired magnitude of 3. The THD for the waveform obtained using the THD block in PSIM was found to be 13.26%. Although this seems high, the reader should keep in mind that in three phase applications all triplen harmonics will be cancelled out giving a lowest order harmonic (LOH) of 11. The THD will now be just 1.81%. Furthermore, the higher order harmonics can easily be filtered out. Figure 5-6 shows the switching angles calculated to remove the 5th and 7th harmonics for a wider range of V_p.

Case 2: Analysis with Varying DC Sources

This section investigates the MCHBI output when the DC source voltages are allowed to vary. For this example, a slightly modified version of the hybrid system presented in chapter 4 is considered. The PWM inverter in the hybrid system is replaced by an MCHBI with three DC sources which consist of battery banks. One of the battery banks is connected and charged by the PFC and the other two banks are assumed to be connected to PV panels via a power converting stage with MPPT. Each battery bank can be assumed to have a nominal voltage of 200V but is normalized to 1V in order to simplify the calculations and discussion. It is assumed that the normalized voltage for a fully charged bank will be 1.1V and a depleted battery will have 0.9V. During grid connection, the PFC charges one of the battery banks and so it is assumed to always be fully charged. The PV panels charge the other two banks and due to the intermittent nature of insolation levels, the bank voltages are allowed to vary from 0.9V to 1.1V. Although the DC source voltage can
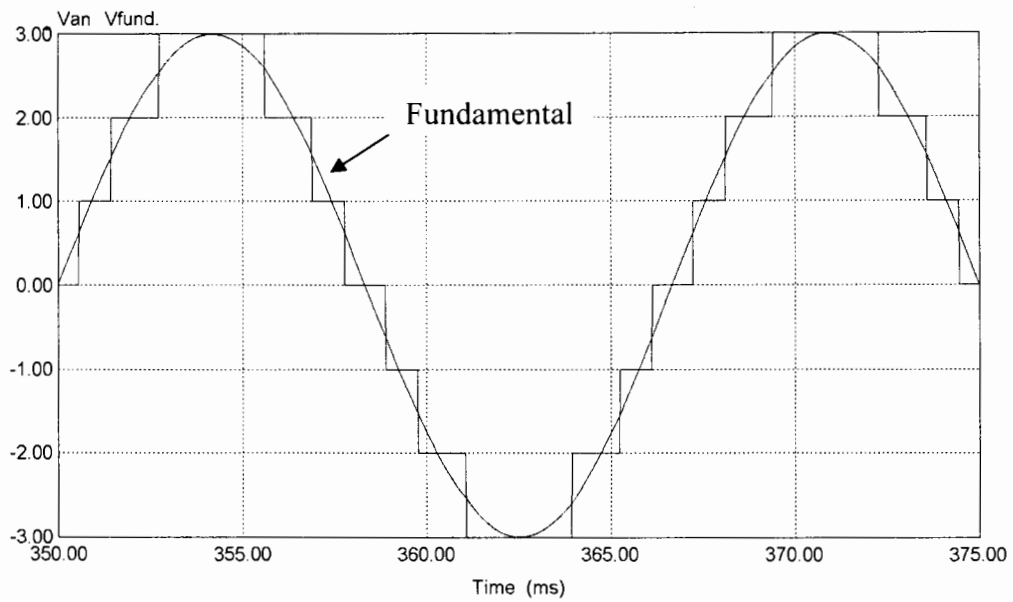
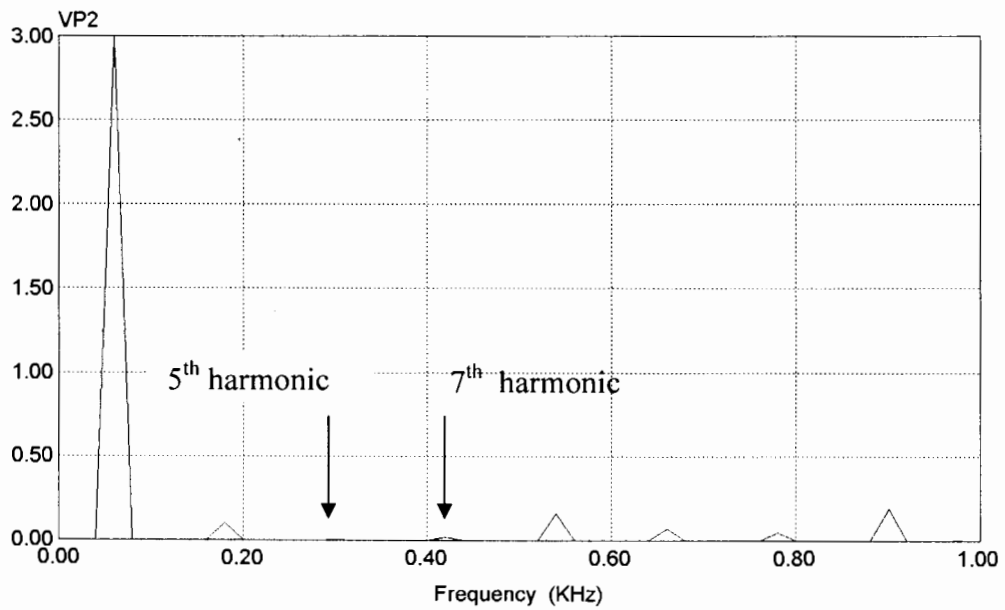*Figure 5-4: Staircase Phase Voltage Waveform with Fundamental Component*

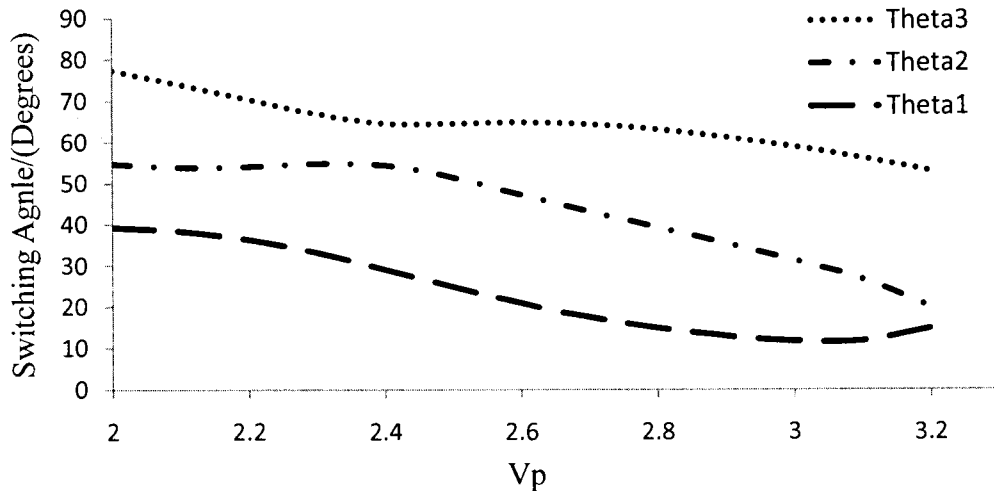*Figure 5-5: FFT of Staircase Waveform*

81

Figure 5-6: Switching Angles Versus V_p for Three-Step Waveform

continuously vary anywhere between 0.9V and 1.1V, only discrete values of 0.9V, 1.0V and 1.1V are chosen in order to simplify the discussion. The three phase AC output from the MCHBI is connected to the rotor windings of the DFIG.

The DFIG windings have a set of leakage and mutual inductances which help to attenuate the harmonics in the voltage induced in the stator. The harmonics are attenuated in a two-step process, first in the current injected into the rotor and then the voltage induced in the stator. The output voltage from the stator contains harmonics which result from the odd harmonics present in the rotor-injected voltage given by (5.1) with $\omega = 2\pi f_r$, and the mechanical frequency (f_m). Thus the stator will have the following harmonics: $5f_r -f_m$, $7f_r + f_m$, $11f_r -f_m$, $13f_r + f_m$, ... [37]. It is desirable to have a higher LOH which is possible if the 5th and 7th harmonics from the MCHBI output are eliminated.

It should be noted that the physical order in which the DC sources are connected does not matter since each H-bridge is independently switched. However, in order to balance the battery use, the switching must take place such that the battery with the highest

voltage has the longest duty cycle and the battery with the lowest voltage has the shortest duty cycle. If the voltage of any one or more of the DC sources changes, the staircase waveform and the harmonic content of the output will also change. Therefore, the switching angles have to be properly determined for each possible arrangement of DC voltage levels in order to selectively eliminate the 5th and 7th harmonics and also achieve the desired magnitude of the fundamental component V_p.

The six possible DC source arrangements are shown in Table 5-3 and the switching angles for each arrangement, calculated for V_p ranging from 2V to about 3.2V, are presented in Figure 5-7. For values outside this range, the numerical algorithm did not converge and no solutions were found to exist. The THD for each arrangement, calculated for $V_p = 3$, is also shown in Table 5-3. Figure 5-8 shows a sample staircase waveform for case # 3 with $V_{PFC} = 1.1$, $V_{PV1} = 0.9$, $V_{PV2} = 0.9$, and $V_P = 3$ where V_{PFC} is DC voltage from the three-phase PFC and V_{PV1}, V_{PV2} are output voltages from selected groups of PV panels. The FFT of the waveform of Figure 5-8 is shown Figure 5-9 and it is seen that the 5th and 7th harmonics have been eliminated and the amplitude of V_P is 3.

The DFIG system shown in Chapter 4 (Figure 4-1) is simulated in PSIM except, this time, the three-phase rotor injection voltage is supplied by a three-phase MCHBI. The three DC sources connected to the H-bridges are equal. Figure 5-10 shows the staircase voltage waveform or the rotor injection voltage (V_{ra}) and the stator output voltage (V_{sa}) for one phase of the machine. The rotor injection frequency is 30 Hz and the stator frequency is 60 Hz. Figure 5-11 shows the FFT of the two waveforms. It is seen that 5th and 7th harmonics in the rotor voltage waveform have been eliminated. The FFT of the stator AC voltage shows negligible harmonics despite the harmonics in the rotor voltage. This is

because the machine inductances help to attenuate the harmonics in the voltage induced in the stator.

Table 5-3: DC Source Arrangements and THD

Case #	V_{PFC}	V_{PV1}	V_{PV2}	THD%
1	1.1	1.1	0.9	12.46
2	1.1	1	0.9	12.49
3	1.1	0.9	0.9	12.61
4	1.1	1.1	1	12.79
5	1.1	1	1	12.87
6	1.1	1.1	1.1	13.26

5.3. Conclusions

This chapter describes multilevel inverters which are gaining increasing attention for use in renewable energy systems. Among the various types of multilevel inverters it is the MCHBI with fundamental frequency switching that is chosen for analysis in this chapter. The MCHBI is a good option for renewable energy applications because they are modular and scalable. Furthermore, low frequency fundamental switching helps to overcome the problems of high frequency switching experienced by PWM VSIs. Analysis is done to show how the switching angles can be selected so that a fundamental voltage component of a desired magnitude can be generated while eliminating certain specifically chosen lower order harmonics. The solution of switching angles requires numerical methods and the Newton-Raphson algorithm is used in this work. The analysis is done for an MCHBI with three DC sources ($s = 3$) for two cases: equal DC sources and varying DC sources. With varying DC sources consisting of batteries, in order to balance the battery use, the inverter switching must take place such that the battery with the highest voltage

84
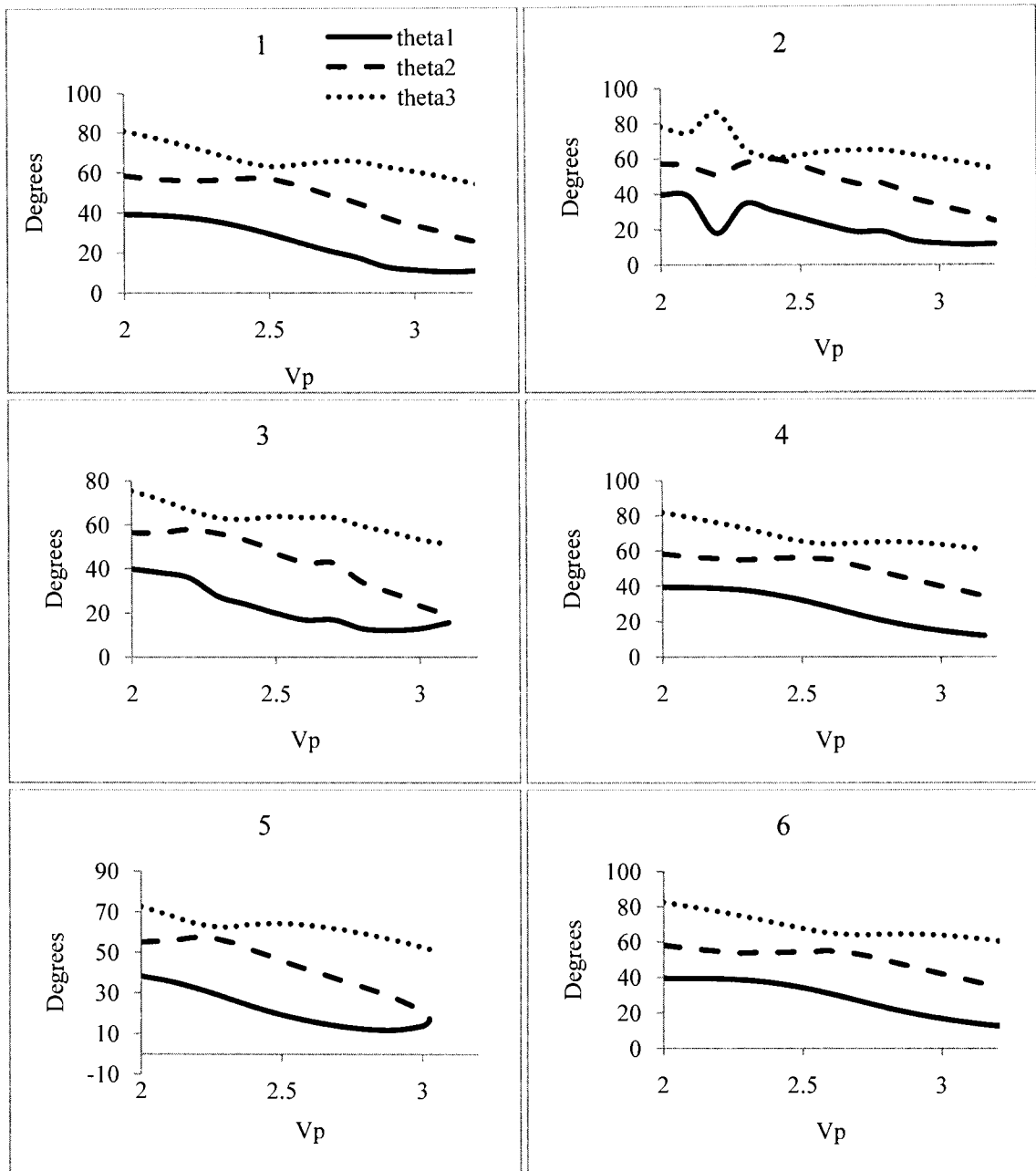
Figure 5-7: Switching Angles Versus V_p for Unequal DC Sources
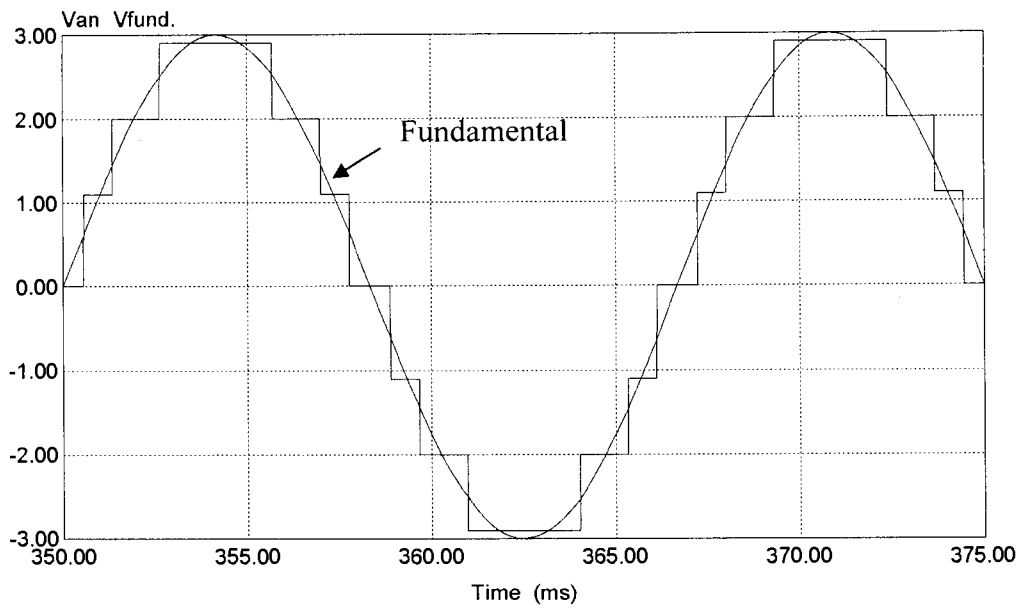
Figure 5-8: Staircase Waveform for $V_{PFC} = 1.1$, $V_{PV1} = 0.9$, $V_{PV2} = 0.9$, $V_P = 3$
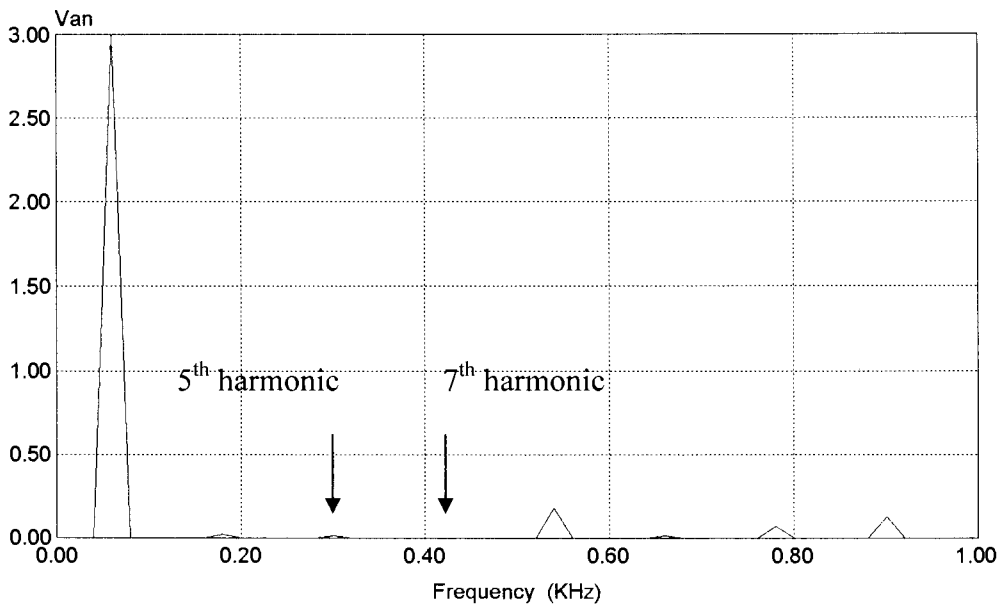
Figure 5-9: FFT for Waveform in Figure 47.
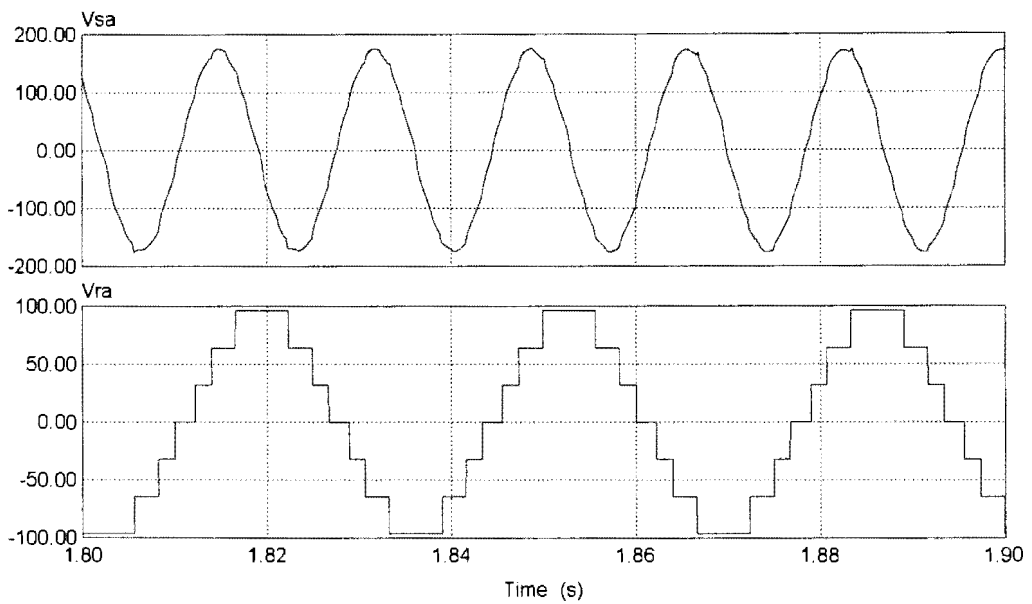
Figure 5-10: Stator (V$_{sa}$) and Rotor Voltage (V$_{ra}$) Waveforms for DFIG
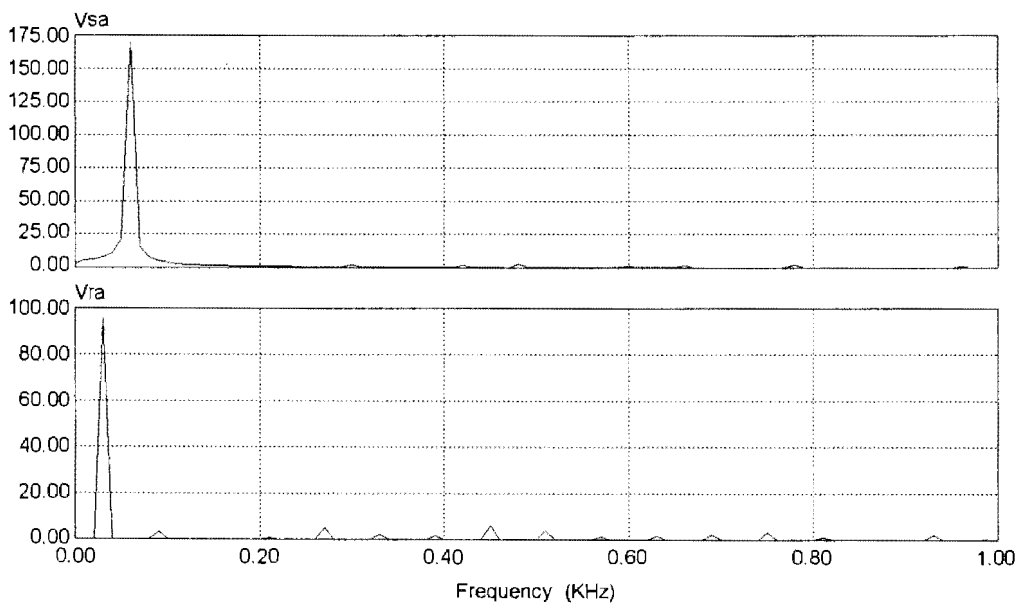
Figure 5-11: FFT of DFIG Rotor and Stator Voltages

has the longest duty cycle and the battery with the lowest voltage has the shortest duty

cycle. Switching angles are computed for both cases such that the 5th and 7th harmonics are

eliminated and a desired magnitude of the fundamental component V$_p$ over a finite range is

obtained. A three-phase MCHBI feeding the rotor of a DFIG is simulated in PSIM and the rotor and stator voltage waveforms are presented. Despite the staircase nature of the waveform used for rotor injection, the stator voltage exhibits negligible distortion.

CHAPTER 6. CONCLUSIONS

6.1. Summary of Work Done

This thesis presents a hybrid DFIG-based wind energy system with an efficient rotor injection scheme with the possibility of providing the injection power from either three-phase AC mains or PV panel-battery combination. The hybrid power converter system proposed is useful in combining wind energy and solar energy such that the wind energy constitutes the bulk of the power produced while the PV panels provide a fraction of the power through rotor excitation. The grid-side AC-DC converter used has features like unity PF, ZVS and high efficiency. The boost converter used to feed PV power to the rotor does not use any additional switches thereby resulting in a simpler power circuit. A current based MPP tracking system is implemented using a DSC to ensure that maximum available power is extracted from the PV panels. A three-phase Sine PWM inverter is used to convert the DC voltage from the three-phase PFC/ PV converter into a variable-frequency AC voltage that is injected into the rotor of the DFIG. In the hybrid system, a Sine PWM based slip control scheme together with constant volts/hertz control is implemented for the rotor-side converter to ensure that the stator voltage of the DFIG is maintained constant. The complete system is first simulated to make sure that the proposed algorithm works well. A DSC based inverter controller for DFIG rotor injection is also experimentally implemented.

This thesis also proposes the concept of utilizing multilevel inverters for DFIG rotor injection. MCHBIs can be useful in combining different DC sources in order to synthesize an AC voltage that can be used for DFIG rotor injection. The sources of DC power could be obtained from a combination of RE sources and also from the grid. The switching angles

can be selected so that a fundamental voltage component of a desired magnitude can be generated while eliminating certain specifically chosen lower order harmonics. A three-phase MCHBI feeding the rotor of a DFIG is simulated in PSIM and the rotor and stator voltage waveforms are presented. Despite the staircase nature of the waveform used for rotor injection, the stator voltage exhibits negligible distortion.

6.2. Future Work

The system proposed in this thesis operates only at sub-synchronous speeds where the inverter injects power into the rotor. Allowing the DFIG to operate at super-synchronous speeds means more energy to be extracted from the wind. At super-synchronous speeds, the grid-side converter can be used as a rectifier and the excess power from the DFIG rotor could be used to charge a battery connected across the DC link. However, if the battery voltage is higher/ lower than the DC link voltage, this might require the addition of another DC/DC converter to the system. Furthermore, a charge controller may be implemented to regulate the battery charging.

Another enhancement that could be made to the hybrid system is to allow an automatic transition between grid-supplied rotor injection or PV rotor injection when grid connection is not possible. In this case, the controller can be made to continuously monitor the grid at the point of common coupling. If the grid fails, the controller can open a breaker connecting the grid to the WES and then close another switch to in order to connect the PV panels to the system.

This thesis has proposed an MCHBI in the hybrid form to provide a three-phase sinusoidal voltage for rotor injection. The MCHBI is powered by three battery banks, one charged by the PFC and the other two charged by PV panels via a power converting stage.

Simulation results showed that the stator voltage of the DFIG had negligible harmonics despite the staircase waveform of the rotor injection voltage. Future work could involve implementing the system in hardware and designing a controller for the MCHBI such that it can provide a variable frequency three-phase injection voltage to the DFIG.

REFERENCES

[1] Munir Kaderbhai and S. Yuvarajan, "Hybrid rotor injection scheme for a doubly fed induction generator," Proceedings of the Symposium on Power Electronics and Machines in Wind Applications (PEMWA), Lincoln, NE, June 2009, pp. 1-4.

[2] F. Blaabjerg and Z. Chen, *Power Electronics for Modern Wind Turbines*, Morgan and Claypool Publishers, San Rafael, CA, 2006.

[3] L. Chang, "Wind energy conversion systems," IEEE Canadian Review, No. 40, p.2, Spring 2002.

[4] G.L. Johnson, *Wind Energy Systems*, Prentice-Hall Inc, Englewood Cliffs, NJ, 2001.

[5] O. Anaya-Lara, N. Jenkins, J. Ekanayake, P. Cartwright and M. Hughes, *Wind Energy Generation: Modeling & Control*, John-Wiley & Sons, Ltd, West Sussex, England, 2009.

[6] T. Ackermann, *Wind Power in Power Systems*, John Wiley & Sons, West Sussex, England, 2005.

[7] S. Muller, M. Deicke, and R.W. De Doncker, "Doubly fed induction generator systems," IEEE Industry Applications Magazine, pp. 26-33, May - June 2002.

[8] National Renewable Energy Labs, "Solar Photovoltaic Technology," [Online]. Available: http://www.nrel.gov. [Accessed: Dec. 27, 2009].

[9] Y. C. Kuo, T. J. Liang and F. C. Chen, "Maximum Power Point Tracking Controller for Photovoltaic Energy Conversion Systems," IEEE Trans. Industrial Electronics, Vol. 48, pp. 594-601, June 2001.

[10] D. Yu, "Power conversion and control methods for renewable energy sources," Ph.D. dissertation, North Dakota State University, Fargo, ND, May 2005.

[11] T. Esram and P. Chapman, "Comparison of photovoltaic array maximum power point tracking techniques," IEEE Trans. on Energy Conv., Vol. 22, No. 2, pp. 439-449, June 2007

[12] Ch. Hua, J. Lin, and Ch. Shen, "Implementation of a DSP-controlled PV system with peak power tracking," IEEE Trans. Ind. Electronic., Vol. 45, No. 1, pp. 99-107, Feb. 1998.

[13] V. Salas, E. Olias, A. Barrado, A. Lazaro, "Review of maximum power tracking algorithms for standalone photovoltaic systems," Solar Energy Materials and Solar Cells, Vol. 90, pp. 1555-1578, January 2006.

[14] S. Yuvarajan and S. Xu, "Photo-voltaic power converter with a simple maximum power point tracker," Proc. 2003 International Sym. on Circuits and Syst., 2003, pp. 399-402.

[15] N. Mohan, *First Course on Power Electronics*, MNPERE, Minneapolis, MN, 2007.

[16] H. De Battista, P. Puleston, R. Mantz and C. Christiansen, "Sliding Mode Control of Wind Energy Systems with DOIG - Power Efficiency and Torsional Dynamics Optimization," IEEE Transactions on Power Systems, Vol. 15, No. 2, pp. 728-734, May 2000.

[17] I. Cardici and M. Ermis, "Double-output induction generator operating at sub-synchronous and super-synchronous speeds: steady-state performance optimization and wind-energy recovery," IEE Proc B Electric Power Applications, pp. 429-42, 1992.

[18] J. Baroudi, V. Dinavahi and A. Knight, "A review of power converter topologies for wind generators," Renewable Energy, Vol. 32, pp. 2369-2385, 2007.

[19] L. Feddersen, E. Siebenthaler, and B. Andresen, "Variable speed wind turbine having a passive grid side rectifier with scalar power control and dependent pitch control," U.S. patent 2004222642, February 8th, 2004.

[20] D. Weng and S. Yuvarajan, "Resonant-boost-input three-phase power factor corrector," IEEE Trans. Power Electronics, Vol. 14, No. 6, , pp. 1149 -1155, Nov. 1999.

[21] H. Mao, D. Boroyevich, A. Ravindra, and F. Lee, "Analysis and design of a high frequency three-phase boost rectifier," IEEE Appl. Power Electronics Conf. and Exposition, 1996, pp. 538-544.

[22] A.R. Prasad, P. D. Ziogas, and S. Manias, "An active power factor correction technique for three phase diode rectifiers," IEEE Trans. on Power Electronics, Vol. 6, No. 1, pp. 58-66, Jan. 1991.

[23] J.M. Enrique, E. Duran, M. Sidrach-de-Cardona and J.M. Andujar, "Theoretical assessment of the maximum power point tracking efficiency of photovoltaic facilities with different converter topologies", Solar Energy, pp. 31–38, 2007.

[24] A. Petersson, L. Harnefor and T. Thiringer, "Evaluation of current control methods for wind turbines using doubly-fed induction machines," IEEE Trans. Power Electronics, Vol. 20, No. 1, pp. 227- 235, Jan. 2005.

[25] L. Helle, "Modeling and comparison of power converters for doubly fed induction generator wind turbines", Ph.D. Thesis, Aalborg University Institute of Energy Technology, Aalborg, Denmark, April 2007.

[26] PSIM, A software by Powersim Technologies, Professional Version 6.05, 2004.

[27] M. Masoum, H. Dehbonei and E.F. Fuchs, "Theoretical and experimental analyses of photovoltaic systems with voltage- and current-based maximum power point tracking," IEEE Trans. Energy Conversion, Vol. 17, No. 4, pp. 514- 522, December 2002.

[28] S. Yuvarajan, D. Yu and S. Xu, "A novel power converter for photovoltaic applications," Journal of Power Sources, Vol. 135, No. 1-2, pp. 327- 331, Sept. 2004.

[29] dsPIC by Microchip Technology, Model: dsPIC 30F2020, Data Sheet, 2006.

[30] N. Mohan, T. Undeland and W. Robbins, *Power Electronics Converters, Applications and Design,* John Wiley & Sons, West Sussex, England, 2003.

[31] L. Fan and S. Yuvarajan, "Modeling and slip control of a doubly fed induction wind turbine," Proceedings of North America Power Symposium, Calgary, Canada, Sept. 2008, pp. 1-6.

[32] F. Sargos, "Application Note AN-8005, IGBT Power Electronics Teaching System Principle for sizing of power converters," Semikron, Hudson, NH, Sept. 2008.

[33] M.H. Rashid, Ed., *Power Electronics Handbook, 2nd Edition: Devices, Circuits and Applications*, Academic Press, San Diego, CA, 2007.

[34] J. Adabi, F. Zare and A. Ghosh, "Analysis of Shaft Voltage in a Doubly-fed Induction Generator," International Conf. on Renewable Energies and Power Quality, Valencia Spain, April 2009, p. 206.

[35] L. M Tolbert and F. Peng, "Multilevel converters as a utility interface for renewable energy systems", IEEE Power Engineering Society Summer Meeting, July 2000, pp. 1271-1274.

[36] L.M. Tolbert, J.N. Chiasson, Z. Du, and K.J. McKenzie, "Elimination of harmonics in a multilevel converter with non-equal DC sources," IEEE Transactions on Industry Applications, Vol. 41, No. 1, Jan./Feb. 2005, pp. 75-82.

[37] S. Yuvarajan and L. Fan, "A doubly-fed induction generation-based wind generation system with quasi-sine rotor injection", Journal of Power Sources, Vol. 184, 2008, pp. 325-330.

LIST OF PUBLICATIONS

1. M. Kaderbhai and S. Yuvarajan, "Hybrid rotor injection scheme for a doubly fed induction generator," Proceedings of the Symposium on Power Electronics and Machines in Wind Applications (PEMWA), Lincoln, NE, June 2009, pp. 1-4.

2. S. Yuvarajan and M. Kaderbhai, "Hybrid renewable energy system with wind turbine and PV panels," IEEE Green Technologies Conference, Grapevine, TX, April 2010.

3. S. Yuvarajan and M. Kaderbhai, "PV-assisted wind energy system with DFIG," First International Conference on Intelligent Design and Analysis of Engineering Products, Systems and Computing, Coimbatore, India, July 2010.